LIGAND DESIGN FOR DEVELOPING F-ELEMENT PHOTOCHEMISTRY

A Thesis
Presented to
The Academic Faculty

by

Brandon Jon Yik

In Partial Fulfillment
of the Requirements for the Degree
Master of Science in the
School of Chemistry and Biochemistry

Georgia Institute of Technology
May 2019

LIGAND DESIGN FOR DEVELOPING F-ELEMENT PHOTOCHEMISTRY

Approved by:

Dr. Henry S. La Pierre, Advisor
School of Chemistry and Biochemistry
Georgia Institute of Technology

Dr. Joseph P. Sadighi
School of Chemistry and Biochemistry
Georgia Institute of Technology

Dr. Z. John Zhang
School of Chemistry and Biochemistry
Georgia Institute of Technology

Date Approved: April 26, 2019

ACKNOWLEDGEMENTS

I would like thank my research advisor, Professor Henry (Pete) La Pierre, for the opportunity to work and learn in his research group. Pete has taught me a good amount about chemistry, the *f*-elements, and what it really means to do air-free and sensitive chemistry. Without his support, I would not be here today. I would like to thank some faculty that have helped oversee my research over the years, Professor Joseph Sadighi, Professor Z. John Zhang, Professor Seth Marder, and Professor Cora MacBeth for their mentorship.

I would like to thank Dr. Leslie Gelbaum and Dr. Johannes Leisen for their patience and guidance in the NMR laboratory. I also thank Dr. John Bacsa for his assistance, mentorship, and collaboration in the X-ray diffraction laboratory.

I have to have a give great thanks for members of the La Pierre group over the years. I would like to thank all my group members for their friendship, humor, advice, and support: Dr. Kai Wang, Thaige Gompa, Natalie Rice, Luis Aguirre Quintana, Ningxin Jiang, Arun Ramanathan, Kirsten Martin, Dominic Russo, Michael Zott, Benjamin Jean, and Tilak Patel. Your friendship and collaborations have been instrumental during my journey.

During my time at Georgia Tech, I have been a teaching assistant during the fall and spring terms. Through this, I have been close to several of those that I have taught with. I am extremely grateful for their encouragement, support, and friendship: Dr. John Tillotson, Dr. Amanda Stephens, Prof. Joseph Sadighi, Dr. Robert Braga, Prof. E. Kent Barefield, Dr. Christy O'Mahony, Dr. Hui Zhu, Dr. Mary

Peek, Dr. Carrie Shepler, Dr. Kimberly Schurmeier, and Dr. Michael Evans. I would also like to thank my fellow teaching assistants for their friendship: Dr. Yu Cao, Dr. Kevin Omolo, Mr. Abraham Jordan, Mr. Eric Drew, and Mr. Christopher Kuehner.

I would especially like to thank Dr. Amanda Stephens and Prof. Angus Wilkinson for the opportunity to teach as co-instructor-of-record for Chem 2380 in Spring 2019 through the Tech to Teaching program. Thank you to Dr. David Lawrence and Dr. Kate Williams from the Center for Teaching and Learning for your mentorship and allowing to be part of this wonderful program.

I thank you to all those in your understanding, encouragement, and support of my decision to pursue my passion in chemical education. To all: thank you for your conversations and advice throughout this experience. It has been of immense help.

I would especially like to thank my family and friends for their unconditional love and support throughout this entire process. None of this would have been possible without you. Thank you!

TABLE OF CONTENTS

LIST OF TABLES

LIST OF FIGURES

LIST OF SCHEMES

LIST OF SYMBOLS AND ABBREVIATIONS

~	Approximately
Å	Angstrom
α	Alpha
β	Beta
γ	Gamma
δ	Chemical Shift
ϵ	Epsilon
ϕ	Quantum Yield
π	Pi-electron
τ	Lifetime
°	Degree(s)
° C	Degree(s) Celsius
%	Percent
Ar	Aryl
ATR	Attenuated Total Reflection
ax	Axial
Bn	Benzyl
bpy	Bipyridine
br	Broad
C	Carbon
C_6D_6	Benzene-d_6

$CDCl_3$	Chloroform-*d*
cent	Centroid
COT	Cyclooctatetraene
Cp*	Pentamethylcyclopentadienyl
CT	Charge Transfer
d	Doublet
dd	Doublet of Doublets
ddd	Doublet of Doublets of Doublets
EDTA	Ethylenediaminetetraacetic Acid
eq	Equivalents or Equatorial
Et	Ethyl
EtOAc	Ethyl Acetate
EtOH	Ethanol
FT	Fourier-Transform
g	Gram(s)
h	Hour(s)
H	Hydrogen
HMPA	Hexamethylphosphoramide
Hz	Hertz
I	Iodide
*i*Pr	Isopropyl
IR	Infrared
K	Kelvin
L	Polypyridyl or 2-Electron Donor
LMCT	Ligand-to-Metal Charge Transfer

Ln	Lanthanide
m	Multiplet
M	Molar
M	Molecular Mass
Me	Methyl
MeOH	Methanol
mer	Meridional
mg	Milligram(s)
MHz	Mega-hertz
mL	Milliliters
MLCT	Metal-to-Ligand Charge Transfer
min	Minute
mm	Millimeters
MMCT	Metal-to-Metal Charge Transfer
mmol	Millimole
mol	Mol
n-BuLi	*n*-Butyllithium
NIR	Near-Infrared
nm	Nanometers
NMR	Nuclear Magnetic Resonance
NNN	Nitrogen-Nitrogen-Nitrogen
O^{t}Bu	*Tert*-butoxide
OEt_2	Diethyl Ether
Ph	Phenyl
pip	Piperidinyl

PNP	Phosphorus-Nitrogen-Phosphorus
ppm	Parts Per Million
ppy	Phenylpyridine
q	Quartet
R^2	Coefficient of Determination
R_f	Retention Factor
rt	Room Temperature
μs	Microsecond(s)
s	Singlet
sept	Septet
sol	Solvent
t	Triplet
td	Triplet of Doublets
T	Temperature
TPPA	Tripyrrolidinophosphoric Acid Triamide
TMEDA	Tetramethylenediamine
TMS	Trimethylsilyl
*t*Bu	Tert-butyl
THF	Tetrahydrofuran
UV	Ultraviolet
vis	Visible
X	Halogen or One-electron Donor
XRD	X-ray Diffraction

SUMMARY

Overall, this thesis describes the synthesis and characterization of ligand architectures to study *f*-element photochemistry. Chapter 1 provides a general overview of photocatalysis and uses and need to develop photochemistry in the lanthanides. Chapter 2 describes efforts into developing new lanthanide starting materials to advance the field in general, but to also provide a wider set of materials available to use in facilitating discoveries across the *f*-block. These new starting materials involve the synthesis and characterization of diethyl ether adducts of trivalent lanthanide iodides. Chapter 3 of this thesis describes the work done on the synthesis of an anionic phenylpyridine ligand to develop lanthanide analogs of commonly used photocatalysts and photosensitizers in the organic methodology community. The synthesis and characterization of the ligand salt and metalation to yield $Cp^*_2Sm(ppy)$ is described. Two appendices are also included which describe synthesis and metalation studies of two other ligand sets, a triamine pincer ligand and an imidophosphorane ligand, that will be used in studying the photochemistry of the lanthanides.

CHAPTER 1. INTRODUCTION

1.1 Photocatalysis

The development of efficient photochemical reactions for energy storage has been a foremost goal of inorganic chemistry for 20 years.[1] Over the past few decades, there has been significant scientific research efforts dedicated to the development of efficient, but also practical, photocatalysis. The most popular and studied photocatalysts include transition-metal photocatalysts. Ru- and Ir-based polypyridyl complexes have been crucial to photoredox catalysis.[2-3] A wide range of powerful methodologies dependent on photosensitizers to provide sufficient driving force to achieve reactive intermediates have been developed.[4-6] These photocatalysts can generate reactive intermediates due to their capability to absorb light and then start electron or energy transfer reactions from the excited states.

The key to a successful molecular photosensitizer is its ability to harvest high-energy blue light (440 nm, 2.82 eV) for reactivity as this is the intensity maximum in the solar spectrum.[5, 7] Commonly used molecular photosensitizers accomplish their photoredox processes exclusively through outer-sphere electron transfer reactions. For example, in catalytic quenching, electrons from the excited state of the photosensitizers are transferred to an acceptor to afford a photochemical reaction. These methodologies are highly limited by what is available. For example, $[Ru(bpy)_3]^{2+}$ (Figure 1.1A), $Ir(ppy)_3$ (Figure 1.1B), and their analogs (bpy = bipyridine and ppy = phenylpyridine) are the most common

photosensitizers used for visible light photoredox catalysis due to their wide commercial availability.[3]

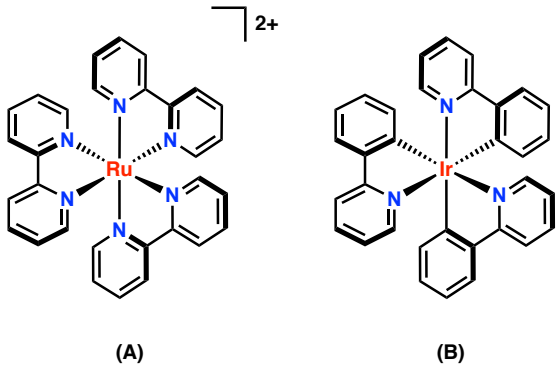

Figure 1.1. Examples of *d*-block metal photosensitizers.

These photosensitizers are also advantageous because of their long excited state lifetime of up to 1,900 ns due to the relaxation of a triplet excited state to a ground state singlet.[8] These singlet-triplet transitions are forbidden and therefore are slow. However, the scope of organic substrates that these photosensitizers can act upon is significantly limited by the redox potentials obtainable by the photoexcited states of these complexes, which are tuned primarily by the substitutions on and derivatizations of the polypyridyl ligand. Modification of the ligand on these transition metal catalysts allows for tuning the excited-state redox properties.[8] Efforts have also focused on extending successes with second and third row transition metals to first row transition metals, such as Fe,[9] Cu,[10] and Cr,[11] and other earth-abundant metals due to their terrestrial availability.[12-13] There has also been some work on using organic photocatalysts

as complimentary reactive species to promote sustainability.[14] Design principles of both earth-abundant metal and organic photocatalysts have been reported.[15-18]

1.2 Lanthanides and Photochemistry

The lanthanides are a group of 15 elements which comprise of lanthanum through lutetium. These elements have been long studied for purposes as luminescent materials.[19] Lanthanides have many advantageous characteristics that can be utilized for photocatalysis but have largely been unexplored in the context of photochemistry. The application of lanthanides has been highly streamlined into the development of sensors[20] and phosphors;[21] however, this is based on *f-f* transitions and the photophysics of lanthanides rather than the photochemistry. Since the lanthanides have terrestrial abundance similar to the late first row transition metals, technologically relevant applications can be envisioned for photochemical energy conversion and storage.[22]

The *f-f* transitions of the lanthanides, like the *d-d* transitions of the transition metals, are Laporte forbidden and thus suffer from low extinction coefficients and quantum yield. However, as with the transition metals, charge transfer – ligand-to-metal (LMCT), metal-to-ligand (MLCT), and in the case of bimetallic systems, metal-to-metal (MMCT) charge transfer – can yield significant absorptivity, quantum yield, and excited state lifetimes. Lanthanides can also be excited by *f-d* transitions, a promotion of an *f*-electron to a higher energy *d*-orbital (Figure 1.2).

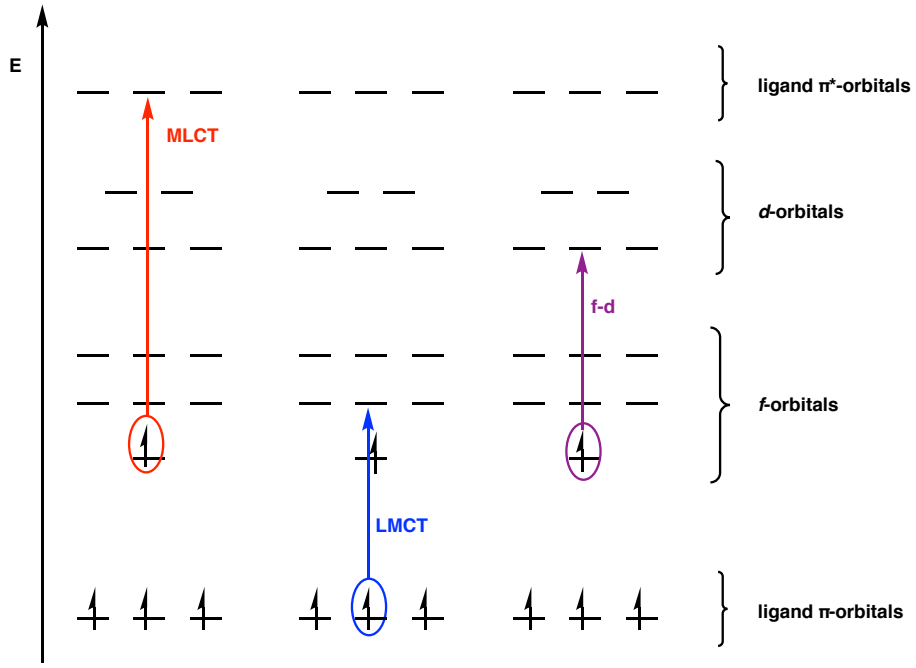

Figure 1.2. Examples of possible electronic transitions in the lanthanides.

These transitions are spin-allowed and can result in highly emissive complexes, common in cerium and praesodymium due to a low *f-d* energy gap.[23] Therefore, it is possible to explore productive photochemistry with lanthanides, given their high molar absorptivity transitions, such as charge transfer and *f-d* transitions. Nevertheless, the lanthanides currently have found few photochemical applications because of their unique synthetic challenges they present. Their limited redox chemistry combined with the confined, core-like nature of the *f*-orbitals make many ligands used in photochemical applications unsuitable. New ligands and alternative synthetic methodologies can be developed to adapt to the preferred coordination geometry and relevant redox potentials of the lanthanides, allowing for the efficient absorption of light with sufficient excited state lifetimes to

perform productive photochemistry for small molecule activation and organic transformations.

1.3 Examples of *f*-Element Photochemistry

There are limited examples of molecular *f*-element photochemistry. Recently, Schelter has reported a cerium(III) *tris*-amide complex displaying an 4*f*-5*d* transitions in the visible region (Scheme 1.1).[24] The strongly reducing character of this ligand set can afford photochemical halogen atom abstraction reactions. Schelter has also shown that the hexachlorocerate(III) anion has been used a potent photoreductant toward aryl chlorides due to the redox active cerium(III) cations behaving like *d*-block-type metalloradicals to engage in single electron transfer (SET) reactions.[25] This work has been further expanded upon to demonstrate the first photoinduced carbon(sp^2)-heteroatom bond forming reaction using a lanthanide as a photoreductant in a photoinduced Miyaura borylation.[26] Schelter has advanced this work looking at the design principles of Ce(III) photocatalysts. They found that complexes with smaller amide ligands showed more reducing potentials, faster electron-transfer rates, and improved efficiency when using a photocatalytic phenylation of an aryl bromide as a model system.

Scheme 1.1. Molecular cerium halogen atom abstraction.

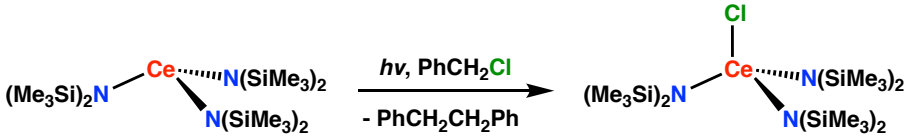

In the early 2000s, Kiplinger synthesized early-actinide pentamethylcyclopentadienyl (Cp*) complexes to study their electronic structure and redox properties.[23] These studies with the actinides have shown that the inclusion of nitrogen-containing ligands (ketimides) contribute to energetically low-lying orbitals. These studies have shown that the incorporation of nitrogen-donor ligands provides for much richer electronic properties compared to halide or alkyl ligands and stabilizes the pentavalent state of uranium. Mixing occurs between the states of the $5f^n$ manifold and the charge transfer states of different parity. There is an enhancement in the *f-f* bands with the ketimide ligand due to an intensity-generating mechanism. The intensity enhancement is proportional the charge transfer transition and is inversely proportional to the energetic separation between the charge transfer states and the *f-f* states. Therefore, as the separation between the *f-f* states and the charge transfer states decreases, there is an increase in *f-f* transition intensity due to low-energy charge transfer transitions that are close in energy to the *f-f* states. Neither the transition intensities nor the transitions, strictly speaking, can be close to the states. This strategy has been used with transition metals to increase the intensity of forbidden *d-d* transitions to generate long-lived excited states.[27] This work has progressed to show that a terminal uranium nitride can be generated by the photolysis of an azide precursor, which releases dinitrogen followed by insertion of the intermediate into the pentamethylcyclopentadienyl ligand C-H bond (Scheme 1.2).[28]

Scheme 1.2. Molecular uranium photolysis.

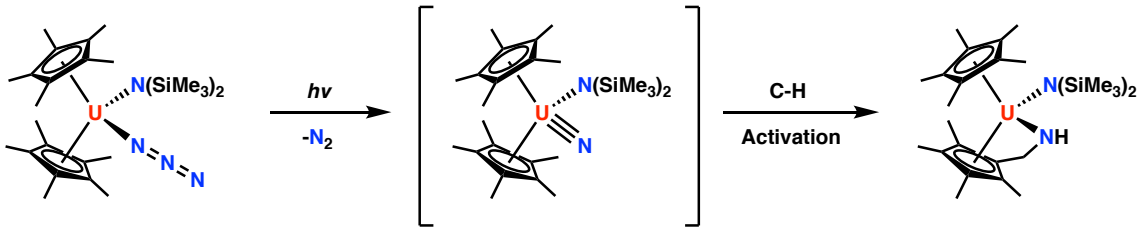

Evans has shown that with an appropriate ligand set, trivalent lanthanide complexes can be photochemically activated leading to a powerful reductive reactivity sufficient to reduce dinitrogen.[29] For example, the heteroleptic *tris*(Cp*) lanthanide complex has low-energy LMCT absorptions that can be photoactivated to reduce dinitrogen (Scheme 1.3).[29] More recently, work has been done to show that photoreductive chemistry is possible with more easily reduced lanthanides based on tailored ligand frameworks for LMCT transitions.[30]

Scheme 1.3. Molecular lanthanide photochemically induced dinitrogen activation.

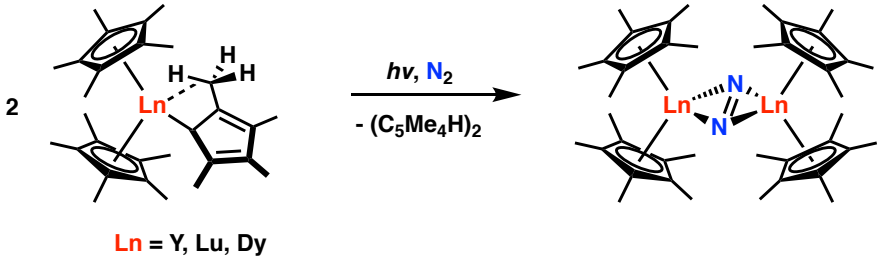

1.4 Applications of Lanthanide Photochemistry

This *f*-element photochemistry has applications in photovoltaics, photoredox organic chemistry, and in photoredox small molecule catalysis. The long-lived excited states of these complexes are desirable since the excited-state

lifetime correlates with the capacity for productive photochemistry. The large redox potentials for photoexcited lanthanide complexes can be employed to improve the efficiency of photovoltaic devices. Tuning these lanthanide chromophores to highly absorb upon the irradiation of visible light will enable powerful photoredox catalysis in a variety of organic transformations. Lanthanide photoredox catalysts can also be coupled to an electrochemical system to create a photoelectrochemical device for chemical energy storage. These *f*-element complexes are also applicable as emissive materials, complementary to sensitized *f-f* luminescent materials for phosphors. The fundamental coordination chemistry and photochemistry described here can be will have a broad impact on several scientific communities and on the use and demand for energy in society. The development of efficient systems for the use of light to power chemical transformations is imperative for a sustainable energy economy.

1.5 References

1. Nocera, D. G., Chemistry of Personalized Solar Energy. *Inorg. Chem.* **2009,** *48*, 10001-10017.

2. Narayanam, J. M.; Stephenson, C. R., Visible Light Photoredox Catalysis: Applications in Organic Synthesis. *Chem. Soc. Rev.* **2011,** *40*, 102-113.

3. Prier, C. K.; Rankic, D. A.; MacMillan, D. W., Visible Light Photoredox Catalysis with Transition Metal Complexes: Applications in Organic Synthesis. *Chem. Rev.* **2013,** *113*, 5322-5363.

4. Nicewicz, D. A.; MacMillan, D. W. C., Merging Photoredox Catalysis with Organocatalysis: The Direct Asymmetric Alkylation of Aldehydes. *Science* **2008,** *322*, 77-80.

5. Schultz, D. M.; Yoon, T. P., Solar Synthesis: Prospects in Visible Light Photocatalysis. *Science* **2014,** *343*, 985.

6. Choi, G. J.; Zhu, Q.; Miller, D. C.; Gu, C. J.; Knowles, R. R., Catalytic Alkylation of Remote C-H Bonds Enabled by Proton-Coupled Electron Transfer. *Nature* **2016,** *539*, 268-271.

7. Ghosh, I.; Ghosh, T.; Bardagi, J. I.; König, B., Reduction of Aryl Halides by Consecutive Visible Light-Induced Electron Transfer Processes. *Science* **2014,** *346*, 725-728.

8. Teegardin, K.; Day, J. I.; Chan, J.; Weaver, J., Advances in Photocatalysis: A Microreview of Visible Light Mediated Ruthenium and Iridium Catalyzed Organic Transformations. *Org. Process. Res. Dev.* **2016,** *20*, 1156-1163.

9. Gualandi, A.; Marchini, M.; Mengozzi, L.; Natali, M.; Lucarini, M.; Ceroni, P.; Cozzi, P. G., Organocatalytic Enantioselective Alkylation of Aldehydes with $[Fe(bpy)_3]Br_2$ Catalyst and Visible Light. *ACS Catalysis* **2015,** *5*, 5927-5931.

10. Kainz, Q. M.; Matier, C. D.; Bartoszewicz, A.; Zultanski, S. L.; Peters, J. C.; Fu, G. C., Asymmetric Copper-Catalyzed C-N Cross-Couplings Induced by Visible Light. *Science* **2016,** *351*, 681-684.

11. Higgins, R. F.; Fatur, S. M.; Shepard, S. G.; Stevenson, S. M.; Boston, D. J.; Ferreira, E. M.; Damrauer, N. H.; Rappe, A. K.; Shores, M. P., Uncovering the Roles of Oxygen in Cr(III) Photoredox Catalysis. *J. Am. Chem. Soc.* **2016,** *138*, 5451-5464.

12. Wenger, O. S., Photoactive Complexes with Earth-Abundant Metals. *J. Am. Chem. Soc.* **2018,** *140*, 13522-13533.

13. Qiao, Y.; Cheisson, T.; Manor, B. C.; Carroll, P. J.; Schelter, E. J., A Strategy to Improve the Performance of Cerium(III) Photocatalysts. *Chem. Commun.* **2019,** *55*, 4067-4070.

14. Romero, N. A.; Nicewicz, D. A., Organic Photoredox Catalysis. *Chem. Rev.* **2016,** *116*, 10075-10166.

15. Joshi-Pangu, A.; Levesque, F.; Roth, H. G.; Oliver, S. F.; Campeau, L. C.; Nicewicz, D.; DiRocco, D. A., Acridinium-Based Photocatalysts: A Sustainable Option in Photoredox Catalysis. *J. Org. Chem.* **2016,** *81*, 7244-7249.

16. Minozzi, C.; Caron, A.; Grenier-Petel, J. C.; Santandrea, J.; Collins, S. K., Heteroleptic Copper(I)-Based Complexes for Photocatalysis: Combinatorial Assembly, Discovery, and Optimization. *Angew. Chem. Int. Ed.* **2018,** *57*, 5477-5481.

17. McCarthy, B. G.; Pearson, R. M.; Lim, C.-H.; Sartor, S. M.; Damrauer, N. H.; Miyake, G. M., Structure−Property Relationships for Tailoring Phenoxazines as Reducing Photoredox Catalysts. *J. Am. Chem. Soc.* **2018,** *140*, 5088-5101.

18. Speckmeier, E.; Fischer, T. G.; Zeitler, K., A Toolbox Approach To Construct Broadly Applicable Metal-Free Catalysts for Photoredox Chemistry: Deliberate Tuning of Redox Potentials and Importance of Halogens in Donor−Acceptor Cyanoarenes. *J .Am. Chem. Soc.* **2018,** *140*, 15353-15365.

19. Bünzli, J.-C. G.; Comby, S.; Chauvin, A.-S.; Vandevyver, C. D. B., New Opportunities for Lanthanide Luminescence. *J. Rare Earths* **2007,** *25*, 257-274.

20. Keefe, M. H.; Benkstein, K. D.; Hupp, J. T., Luminescent Sensor Molecuels Based on Coordinated Metals: A Review of Recent Developments. *Coord. Chem. Rev.* **2000,** *205*, 201-228.

21. Qin, X.; Liu, X.; Huang, W.; Bettinelli, M.; Liu, X., Lanthanide-Activated Phosphors Based on 4f-5d Optical Transitions: Theoretical and Experimental Aspects. *Chem. Rev.* **2017,** *117*, 4488-4527.

22. Haxel, G. B.; Hedrick, J. B.; Orris, G. J., Rare Earth Elements - Critical Resources for High Technology, Fact Sheet 087-02. Survey, U. S. G., Ed. 2005.

23. Morris, D. E.; Da Re, R. E.; Jantunen, K. C.; Castro-Rodriguez, I.; Kiplinger, J. L., Trends in Electronic Structure and Redox Energetics for Early-Actinide Pentamethylcyclopentadienyl Complexes. *Organometallics* **2004,** *23*, 5142-5133.

24. Yin, H.; Carroll, P. J.; Anna, J. M.; Schelter, E. J., Luminescent Ce(III) Complexes as Stoichiometric and Catalytic Photoreductants for Halogen Atom Abstraction Reactions. *J. Am. Chem. Soc.* **2015,** *137*, 9234-9237.

25. Yin, H.; Jin, Y.; Hertzog, J. E.; Mullane, K. C.; Carroll, P. J.; Manor, B. C.; Anna, J. M.; Schelter, E. J., The Hexachlorocerate(III) Anion: A Potent, Benchtop Stable, and Readily Available Ultraviolet A Photosensitizer for Aryl Chlorides. *J. Am. Chem. Soc.* **2016,** *138*, 16266-16273.

26. Qiao, Y.; Yang, Q.; Schelter, E. J., Photoinduced Miyaura Borylation by a Rare-Earth-Metal Photoreductant: the Hexachlorocerate(III) Anion. *Angew. Chem. Int. Ed.* **2018,** *57*, 10999-11003.

27. Raj, G., *Advanced Inorganic Chemistry - II*. 12th ed.; GOEL Publishing House: Meerut, 2010.

28. Thomson, R. K.; Cantat, T.; Scott, B. L.; Morris, D. E.; Batista, E. R.; Kiplinger, J. L., Uranium Azide Photolysis Results in C-H Bond Activation and Provides Evidence for a Terminal Uranium Nitride. *Nat. Chem.* **2010,** *2*, 723-729.

29. Fieser, M. E.; Bates, J. E.; Ziller, J. W.; Furche, F.; Evans, W. J., Dinitrogen Reduction via Photochemical Activation of Heteroleptic Tris(cyclopentadienyl) Rare-Earth Complexes. *J. Am. Chem. Soc.* **2013,** *135*, 3804-3807.

30. Fieser, M. E.; Johnson, C. W.; Bates, J. E.; Ziller, J. W.; Furche, F.; Evans, W. J., Dinitrogen Reduction, Sulfur Reduction, and Isoprene Polymerization via Photochemical Activation of Trivalent Bis(cyclopentadienyl) Rare-Earth-Metal Allyl Complexes. *Organometallics* **2015,** *34*, 4387-4393.

CHAPTER 2. LANTHANIDE STARTING MATERIALS

2.1 Note on Collaboration

This chapter is based on collaborative research efforts currently under review for publication. All authors (Thaige P. Gompa, Natalie T. Rice, Dominic R. Russo, Luis M. Aguirre Quintana, John Bacsa and Henry S. La Pierre) agree to the description of the work as a whole in this Master's Thesis and the reuse of images herein. The synthetic work contributed by Brandon Yik is detailed in the Experimental section.

2.2 Background

Starting material development is important to the synthesis and discovery of new *f*-block complexes. Recent interests in the *f*-block include single-molecule magnets[1-8] and low-valent transuranic complexes.[9-12] The discovery and development of new lanthanide and actinide starting materials is necessary to further develop these fields. The development of new lanthanide complexes will also aid in the synthesis of new transuranic complexes. Trivalent lanthanides are the closest analogs to trivalent transuranic metals. This is due to similar ionic radii of the lanthanides and actinides. For example, Nd^{3+} (1.01 Å) would be a representative analog for Np^{3+} (1.01 Å).[13] Metal iodide starting materials are common in actinide chemistry and thus it would be important to elucidate the synthesis of lanthanide iodide complexes.[14]

There is literature precedence for lanthanide triiodides both in solution. Syntheses in solution involve reaction of lanthanide (Ln) oxides or metal with hydroiodic acid followed by dehydration with ammonium iodide.[15] Additional syntheses involve the reaction of Ln oxides with ammonium iodide at high temperatures[16-17] and Ln metal with iodine, diiodoethane or iodoform.[18-23] A number of reports include the preparation of *f*-block starting material complexes in low-polarity solvents, including diethyl ether, to access low-coordinate and low-valent *f*-block complexes.[14, 24-25] These materials can then be solvated in THF that can be easily crystallized in two primarily useful forms: $LnI_3(THF)_4$ (Ln = La, Ce, Pr) and as the mixed salt $[LnI_2(THF)_5][LnI_4(THF)_2]$ (Ln = Nd, Sm, Gd, Dy, Er, Tm, Yb).[21, 26-27] From here, these lanthanide iodide tetrahydrofuran adducts can be used in metalation reactions or be derivatized to make other starting materials such as $Ln[N(TMS)_2]_3$,[28] $LnBn_3$,[29] and $LnCp^*_3$.[30]

2.3 Results and Discussion

2.3.1 Synthesis of $LnI_3(OEt_2)_x$

The syntheses of the diethyl ether complexes of lanthanide triiodides begin with treating lanthanide metal turnings or power (up to gram-scale) with a faintly substoichiometric amount of iodine (<1.5 eq) in diethyl ether. The substoichiometric amount of iodine is crucial to avoid formation of red-brown $[I_3]^-$. The mixture was stirred for 4 days, yielding the diethyl ether complex, $LnI_3(OEt_2)_x$. The material was isolated on a sintered glass fritted funnel and washed with diethyl ether to remove any possible residual iodine solution. The solid material may

contain any residual metal and must be mechanically removed before the material can undergo further reactions. In addition, because of the different degrees of partial solvation by diethyl ether, each batch of material must be subject to elemental analysis to determine the amount of coordinated diethyl ether. This is important in reactions that require precise stoichiometric control.

Scheme 2.1. Two-step synthesis of **2-Ln** and **3-Ln** via diethyl ether adduct, **1-Ln**. Lanthanides depicted in red are structurally characterized as **1-Ln** and yields are given over two-steps.

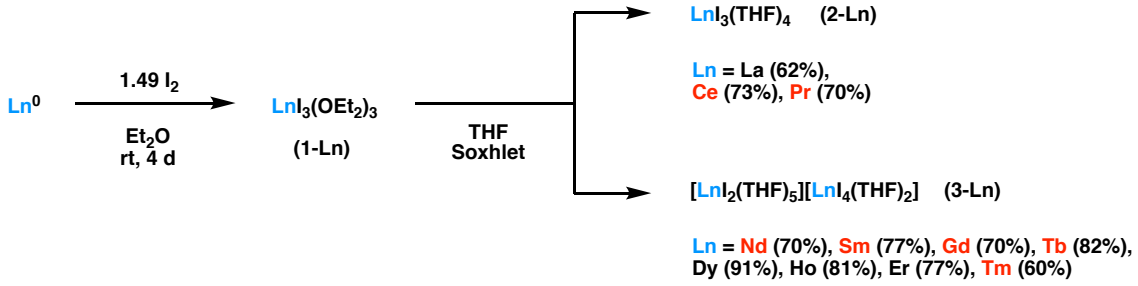

2.3.2 X-ray Crystal Structures of $TbI_3(OEt_2)_3$ and $TmI_3(OEt_2)_3$

Single crystal X-ray diffraction data was obtained for Ln = Ce, Pr, Nd, Sm, Gd, Tb, Tm. The author synthesized and obtained crystal data for **1-Tb** whereas the data for other **1-Ln** complexes were obtained by other members of the group. X-ray diffraction quality single crystals were grown from a concentrated solution of **1-Ln** at -35 °C. These lanthanide triiodide diethyl ether adducts take on a pseudo-octahedral geometry with meridional orientation of the iodides and diethyl ether molecules. The crystal structure of **1-Tb**, TbI_3(*mer*-$OEt_2)_3$, is shown in Figure 2.1.

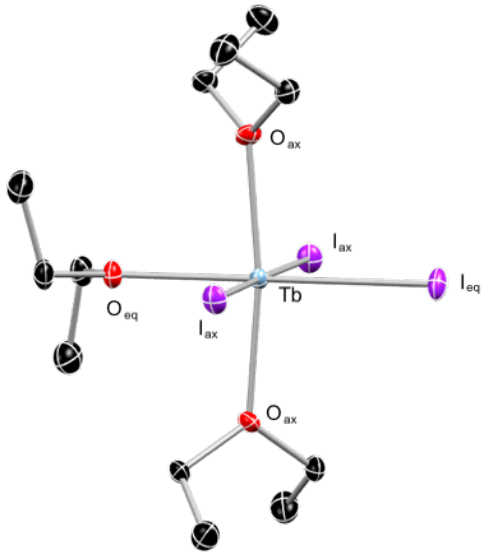

Figure 2.1. Molecular structure of **1-Tb** with thermal ellipsoids shown at 50% probability. H atoms are omitted for clarity.

This complex is isostructural to other **1-Ln** complexes crystallographically characterized by our group (Ln = Ce, Pr, Nd, Sm, Gd, Tb, Tm). The majority of these complexes crystallize in the Pbcn space group (Ln = Ce, Pr, Sm, Gd, Tb), however, **1-Nd** and **1-Tm** deviate and crystallize in the $Pna2_1$ and P-1 space groups, respectively. Data collected for **1-Tm** also does not give suitable refinement, although connectivity can be confirmed. These different space groups show the soft potential that these complexes have for crystallization and that there is sensitivity to diethyl ether ligand loss.

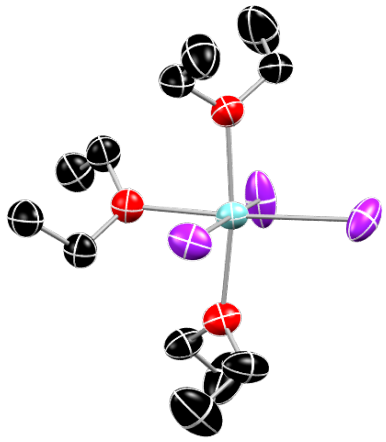

Figure 2.2. Molecular structure of **1-Tm** with thermal ellipsoids shown at 50% probability. H atoms are omitted for clarity.

The crystal structure of **1-Tb** shows a pseudo-octahedral metal center that is coordinated by two axial iodides and one equatorial iodide, along with three meridional diethyl ether molecules. The I_{ax}-Tb-I_{ax} bond angle is 177.822(9)° and the I_{ax}-Tb-I_{eq} bond angles are both 88.911(4)°. The Tb-I_{ax} bond lengths are both 3.0004(3) Å and the Tb-I_{eq} bond length is 2.9706(4) Å.

The Ln-I bond length for the structurally characterized complexes in the Pbcn space group can be compared with the lanthanide's ionic radius. This would demonstrate the effect of lanthanide ion contraction moving across the series. Figure 2.3 shows this trend as metal ionic radius decreases, so does the equatorial Ln-I bond length. The linear fit is great, with an R^2 value of 0.99, meaning that the linear model fits the data very well, with a slope of 1.0764. The y-intercept in this model is 1.975, which represents the ionic radius of an iodide anion. This value is slightly shorter than the Shannon ionic radius for iodide, 2.2 Å.[13] Overall, this model is consistent with structural implications of ionic bonding.[31]

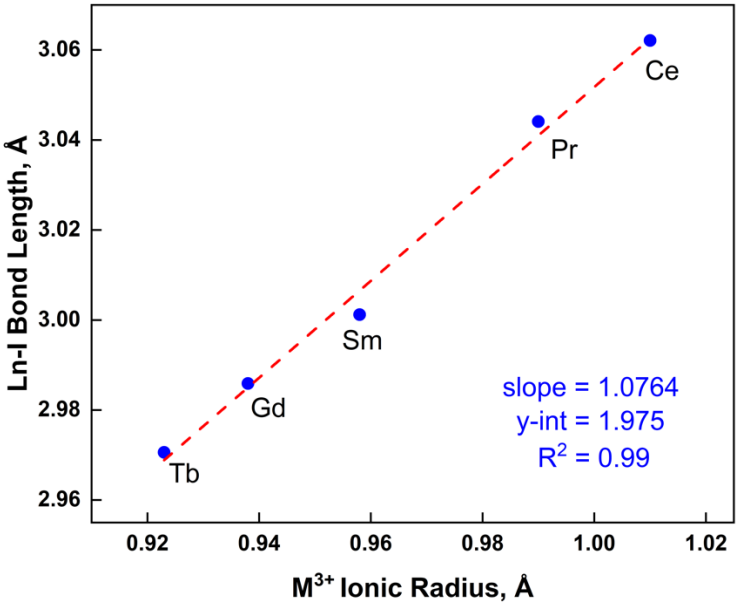

Figure 2.3. Plot of the equatorial Ln-I bond distance relative to the trivalent metal ionic radii in the Pbcn space group.

2.3.3 Synthesis and Characterization of $LnI_3(THF)_x$

Tetrahydrofuran adducts of the lanthanide triiodides are obtained by Soxhlet extraction of the $LnI_3(OEt_2)_x$ material with THF. An advantage of a Soxhlet extraction versus using the diethyl ether adduct is that residual metal and metal oxide are left on the sintered glass frit of the thimble in the apparatus and the THF adducts are more well-defined. Early lanthanides form THF adducts as a neutral species in the form of $LnI_3(THF)_4$ (Ln = La, Ce, Pr), whereas the late lanthanides form adducts as a charge-separated species, $[LnI_2(THF)_5][LnI_4(THF)_2]$ (Ln = Nd, Sm, Gd, Tb, Dy, Ho, Er, Tm). This two-step process of first synthesizing the diethyl ether adduct then converting it to the THF adduct gives good to excellent yields (60-91%). The structure (neutral or charge-separated) of the THF adduct was

established by comparison of the lattice parameters with known structures.[21, 26-27] The charge-separated terbium triiodide THF adduct has not been previously reported and is structurally characterized here.

Lanthanide metal content of **2-Ln** and **3-Ln** were determined by complexometric titration using the disodium salt of ethylenediaminetetraacetic acid (EDTA).[32] A buffer solution was made using hexamethylenetetramine as the buffer and Xylenol Orange as the indicator. Roughly 20-70 mg of either **2-Ln** or **3-Ln** was dissolved in the buffer solution. Then, a 0.15022 M solution of EDTA in H_2O was used to titrate the sample. EDTA binds to lanthanides to form a 1:1: Ln-EDTA complex. The endpoint of the titration is determined visually, when the solution changes color to yellow, signaling that the end-point has been reached. Titrations for each metal complex was completed in triplicate over a range of metal complex masses and the averages of the triplicate are reported in Table 2.1. Overall, the complexometric titration gave good results for the lanthanide metal content found in **2-Ln** and **3-Ln**, with the largest difference of 0.24% for **2-Ce** but only a 0.02% difference for **3-Dy**.

Table 2.1. Lanthanide metal content of **2-Ln** and **3-Ln** found by complexometric titration.

Complex	Found Metal %	Required Metal %
2-La	17.34	17.19
2-Ce	17.55	17.31
2-Pr	17.49	17.40
3-Nd	18.61	18.56
3-Sm	19.31	19.19
3-Gd	19.78	19.90
3-Tb	20.10	20.06
3-Dy	20.45	20.43
3-Ho	20.52	20.65
3-Er	20.99	20.90
3-Tm	21.48	21.06
3-Yb	21.31	21.45

2.3.4 X-ray Crystal Structure of $[TbI_2(THF)_5][TbI_4(THF)_2]$

The charge-separated terbium triiodide THF adduct was synthesized as outlined above, through the Soxhlet extraction of the $LnI_3(OEt_2)_x$ residue with THF. Crystallization from a concentrated solution of **3-Tb** at room temperature yielded single colorless prism-shaped crystals of $[TbI_2(THF)_5][TbI_4(THF)_2]$. The molecular structure of **3-Tb** is shown in Figure 2.4. **3-Tb** crystallizes as ion pairs with the same structural motif as the previously reported analogous, smaller lanthanide complexes (Ln = Nd, Sm, Gd, Yb).[21, 26-27] The cation assumes a slightly distorted

pentagonal bipyramidal geometry with two axial, *trans* iodides and four equatorial THF molecules. The anion adopts an octahedral geometry with two axial THF molecules and four equatorial iodides.

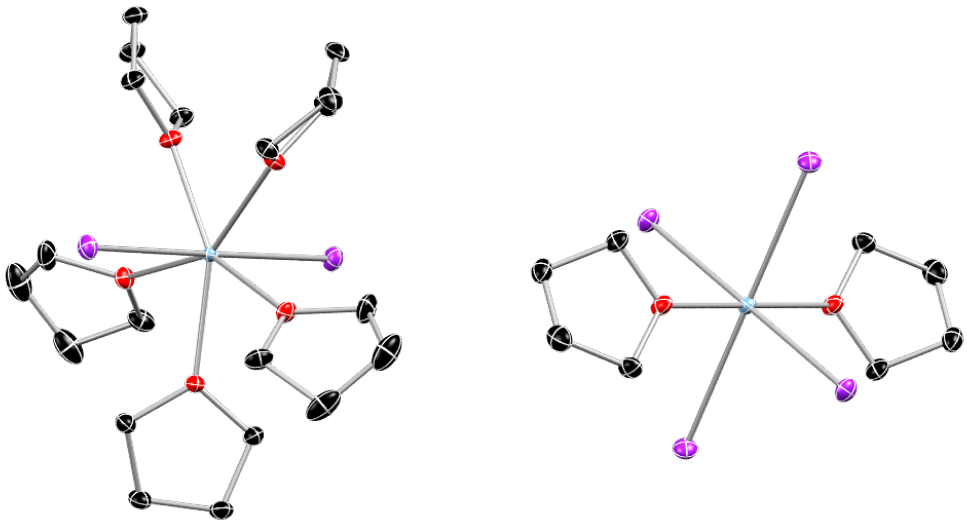

Figure 2.4. Molecular structure of **3-Tb** with thermal ellipsoids shown at 50% probability. H atoms are omitted for clarity.

2.4 Conclusion

In summary, the synthesis for diethyl ether adducts of trivalent lanthanide complexes, $[LnI_3(mer\text{-}OEt_2)_3]$, with the exception of Ln = Pm and Eu, has been achieved. Structural information for Ln = Ce, Pr, Nd, Sm, Gd, Tb, and Tm has been obtained, with Ln = Tb and Tm being reported here. These starting materials can be converted to the well-defined THF adducts and with the structural characterization of $[TbI_2(THF)_5][TbI_4(THF)_2]$, expanding the previously characterized set of known THF adducts.

2.5 Experimental

2.5.1 General Considerations

Unless otherwise noted, all reagents were obtained from commercial suppliers and the syntheses and manipulations were conducted under argon with exclusion of oxygen and water using Schlenk techniques or in an inert atmosphere box (Vigor) under a dinitrogen (<0.1 ppm O_2/H_2O) atmosphere. The glovebox is equipped with two -35 °C freezers. All glassware and cannulae were stored in an oven over-night (>8 h) at a temperature of ca. 160 °C. Celite and molecular sieves were dried under vacuum at a temperature >250 °C for a minimum of 24 h. Diethyl ether and tetrahydrofuran were purged with UHP-grade argon (Airgas) and passed through columns containing Q-5 and molecular sieves in a solvent purification system (JC Meyer Solvent Systems). All solvents in the glovebox were stored in bottles over 3 Å molecular sieves. X-ray structural determinations were performed at the Georgia Institute of Technology on a Bruker D8 Venture diffractometer.

2.5.2 Synthetic Procedures

2.5.2.1 $TbI_3(OEt_2)_3$ (**2-Tb**)

To a slurry of terbium powder (0.4020 g, 2.529 mmol, 1.0 eq) in 20 mL of diethyl ether in a 100 mL Schlenk flask was added a solution of iodine (0.4960 g, 3.769 mmol, 1.49 eq) in diethyl ether (15 mL). The reaction mixture was stirred for 4 days at rt while a tan solid precipitated. The solid was isolated on a fine porosity, sintered glass frit and washed with diethyl ether (2 x 50 mL). The solid was dried *in vacuo* for several hours to yield a free flowing, white microcrystalline powder

(1.4645 g). The precise composition of $TbI_3(OEt_2)_x$ depends on duration of exposure to vacuum.

2.5.2.2 $[TbI_2(THF)_5][TbI_4(THF)_2]$ (**3-Tb**)

$TbI_3(OEt_2)_x$ (1.4645 g) is subjected to Soxhlet extraction with THF yielding a white powder (1.1205 g, 56% over two-steps). Found: Tb, 20.10%. $[TbI_2(THF)_5][TbI_4(THF)_2]$ requires 20.06%.

2.5.3 X-ray Diffraction Data

2.5.3.1 $TbI_3(OEt_2)_3$

Experimental. Single colorless prism-shaped crystals of $TbI_3(OEt_2)_3$ were crystallized from a concentrated solution of diethyl ether at -35 °C. A suitable crystal 0.747×0.60×0.15 mm^2 was selected and mounted on a loop with paratone oil on a Bruker D8 Venture diffractometer with MO Kα radiation and PHOTON II detector. The crystal was kept at 100(2) K during data collection. Using Olex2,[33] the structure was solved with ShelXT[34] structure solution program using Intrinsic Phasing and refined with ShelXL[35] refinement package using Least Squares Minimization.

Crystal Data. $C_{12}H_{30}I_3O_3Tb$ (M = 761.98 g/mol): monoclinic, space group Pbcn (no. 60), a = 10.0273(6) Å, b = 13.7816(9) Å, c = 15.7910(11) Å, V = 2182.2(2) $Å^3$, Z = 4, T = 100(2) K, μ(Mo Kα) = 7.487 mm^{-1}, *Dcalc* = 2.319 g/cm^3, 45138 reflections measured (5.024° ≤ 2θ ≤ 61.016°), 3344 unique (R_{int} = 0.0606, R_{sigma} = 0.0260) which were used in all calculations. The final R_1 was 0.0235 (I > 2σ(I)) and wR_2 was 0.0571 (all data).

3.5.3.2 $[TbI_2(THF)_5][TbI_4(THF)_2]$

Experimental. Single colorless prism-shaped crystals of $[TbI_2(THF)_5][TbI_4(THF)_2]$ were crystallized from a concentrated solution of THF at room temperature. A suitable crystal 0.183×0.124×0.109 mm^2 was selected and mounted on a loop with paratone oil on a Bruker D8 Venture diffractometer with MO Kα radiation and PHOTON II detector. The crystal was kept at 100(2) K during data collection. Using Olex2,[33] the structure was solved with ShelXT[34] structure solution program using Intrinsic Phasing and refined with ShelXL[35] refinement package using Least Squares Minimization.

Crystal Data. $C_{28}H_{56}I_6O_7Tb_2$ (M = 1583.96 g/mol): monoclinic, space group C2/c (no. 15), a = 12.742(3) Å, b = 12.016(3) Å, c = 28.632(6) Å, β = 98.442(4)°, α = γ = 90°, V = 4336.3(16) $Å^3$, Z = 4, T = 100(2) K, μ(Mo Kα) = 7.542 mm^{-1}, *Dcalc* = 2.426 g/cm^3, 35946 reflections measured (2.342° ≤ 2θ ≤ 33.139°), 8278 unique (R_{int} = 0.0486, R_{sigma} = 0.0393) which were used in all calculations. The final R_1 was 0.0283 (I > 2σ(I)) and wR_2 was 0.0618 (all data).

2.6 References

1. Mills, D. P.; Moro, F.; McMaster, J.; van Slageren, J.; Lewis, W.; Blake, A. J.; Liddle, S. T., A Delocalized Arene-Bridged Diuranium Single-Molecule Magnet. *Nat. Chem.* **2011,** *3*, 454-460.

2. King, D. M.; Tuna, F.; McMaster, J.; Lewis, W.; Blake, A. J.; McInnes, E. J.; Liddle, S. T., Single-Molecule Magnetism in a Single-Ion Triamidoamine Uranium(V) Terminal Mono-Oxo Complex. *Angew. Chem. Int. Ed.* **2013,** *52*, 4921-4924.

3. Chilton, N. F.; Goodwin, C. A.; Mills, D. P.; Winpenny, R. E., The First Near-Linear Bis(amide) f-Block Complex: a Blueprint for a High Temperature Single Molecule Magnet. *Chem. Commun.* **2015,** *51*, 101-103.

4. Arnold, P. L.; Cowie, B. E.; Suvova, M.; Zegke, M.; Magnani, N.; Colineau, E.; Griveau, J. C.; Caciuffo, R.; Love, J. B., Axially Symmetric U-O-Ln- and U-O-U-Containing Molecules from the Control of Uranyl Reduction with Simple f-Block Halides. *Angew. Chem. Int. Ed.* **2017,** *56*, 10775-10779.

5. Goodwin, C. A. P.; Ortu, F.; Reta, D.; Chilton, N. F.; Mills, D. P., Molecular Magnetic Hysteresis at 60 Kelvin in Dysprosocenium. *Nature* **2017,** *548*, 439-442.

6. Gould, C. A.; Darago, L. E.; Gonzalez, M. I.; Demir, S.; Long, J. R., A Trinuclear Radical-Bridged Lanthanide Single-Molecule Magnet. *Angew. Chem. Int. Ed.* **2017,** *56*, 10103-10107.

7. Hilgar, J. D.; Flores, B. S.; Rinehart, J. D., Ferromagnetic Coupling in a Chloride-Bridged Erbium Single-Molecule Magnet. *Chem. Commun.* **2017,** *53*, 7322-7324.

8. Guo, F.-S.; Day, B. M.; Chen, Y.-C.; Tong, M.-L.; Mansikkamäki, A.; Layfield, R. A., Magnetic Hysteresis up to 80 Kelvin in a Dysprosium Metallocene Single-Molecule Magnet. *Science* **2018,** *362*, 1400-1403.

9. Dutkiewicz, M. S.; Apostolidis, C.; Walter, O.; Arnold, P. L., Reduction Chemistry of Neptunium Cyclopentadienide Complexes: From Structure to Understanding. *Chem. Sci.* **2017,** *8*, 2553-2561.

10. Windorff, C. J.; Chen, G. P.; Cross, J. N.; Evans, W. J.; Furche, F.; Gaunt, A. J.; Janicke, M. T.; Kozimor, S. A.; Scott, B. L., Identification of the Formal +2 Oxidation State of Plutonium: Synthesis and Characterization of $\{Pu(II)[C_5H_3(SiMe_3)_2]_3\}^-$. *J. Am. Chem. Soc.* **2017,** *139*, 3970-3973.

11. Su, J.; Windorff, C. J.; Batista, E. R.; Evans, W. J.; Gaunt, A. J.; Janicke, M. T.; Kozimor, S. A.; Scott, B. L.; Woen, D. H.; Yang, P., Identification of the Formal +2 Oxidation State of Neptunium: Synthesis and Structural Characterization of $\{NpII[C_5H_3(SiMe_3)_2]_3\}^{1-}$. *J .Am. Chem. Soc.* **2018,** *140*, 7425-7428.

12. Galley, S. S.; Sperling, J. M.; Windorff, C. J.; Zeller, M.; Albrecht-Schmitt, T. E.; Bart, S. C., Conversion of Americia to Anhydrous Trivalent Americium Halides. *Organometallics* **2019,** *38*, 606-609.

13. Shannon, R. D., Revised Effective Ionic Radii and Systematic Studies of Interatomic Distances in Halides and Chalcogenides. *Acta Cryst.* **1976,** *A32*, 751-767.

14. Windorff, C. J.; Dumas, M. T.; Ziller, J. W.; Gaunt, A. J.; Kozimor, S. A.; Evans, W. J., Small-Scale Metal-Based Syntheses of Lanthanide Iodide, Amide, and Cyclopentadienyl Complexes as Analogues for Transuranic Reactions. *Inorg. Chem.* **2017,** *56*, 11981-11989.

15. Young, R. C.; Hastings, J. L., Reaction of Lanthanum Oxide with Ammonium Iodide. *J. Am. Chem. Soc.* **1937,** *59*, 765-766.

16. Taylor, M. D.; Carter, C. P., Preparation of Anhydrous Lanthanide Halides, Especially Iodides. *J. Inorg. Nucl. Chem.* **1962,** *24*, 387-391.

17. Boyle, T. J.; Ottley, L. A.; Alam, T. M.; Rodriguez, M. A.; Yang, P.; McIntyre, S. K., Structural Characterization of Methanol Substituted Lanthanum Halides. *Polyhedron* **2010,** *29*, 1784-1795.

18. Bruno, G.; Ciliberto, E.; Fischer, R. D.; Fragala, I.; Spiegl, A. W., Photoelectron Spectroscopy of f-Element Organometallic Complexes. V. Comparative Study of Ring-Substituted Uranocenes. *Organometallics* **1982,** *1*, 1060-1062.

19. Deacon, G. B.; Feng, T.; Junk, P. C.; Meyer, G.; Scott, N. M.; Skelton, B. W.; White, A. H., Structural Variety in Solvated Lanthanoid(III) Halide Complexes. *Aust. J. Chem.* **2000,** *53*, 853-865.

20. Lannou, M.-I.; Hélion, F.; Namy, J.-L., Some Uses of Mischmetall in Organic Synthesis. *Tetrahedron* **2003,** *59*, 10551-10565.

21. Izod, K.; Liddle, S. T.; Clegg, W., A Convenient Route to Lanthanide Triiodide THF Solvates. Crystal Structures of $LnI_3(THF)_4$ [Ln = Pr] and $LnI_3(THF)_{3.5}$ [Ln = Nd, Gd, Y]. *Inorg. Chem.* **2004,** *43*, 214-218.

22. Huebner, L.; Kornienko, A.; Emge, T. J.; Brennan, J. G., Heterometallic Lanthanide Group 12 Metal Iodides. *Inorg. Chem.* **2004,** *43*, 5659-5664.

23. Kunze, M. R.; Steinborn, D.; Merzweiler, K.; Wagner, C.; Sieler, J.; Taube, R., Synthese, Struktur und Reaktivität von Tris-, Bis- und Mono(2,4-dimethylpentadienyl)-Komplexen des Neodyms, Lanthans und des Yttriums. *Z. Anorg. Allg. Chem.* **2007,** *633*, 1451-1463.

24. Natrajan, L.; Mazzanti, M.; Bezombes, J.-P.; Pécaut, J., Practical Synthetic Routes to Solvates of $U(OTf)_3$: X-ray Crystal Structure of $[U(OTf)_3(MeCN)_3]_n$, a Unique U(III) Coordination Polymer. *Inorg. Chem.* **2005,** *44*, 6115-6121.

25. Carmichael, C. D.; Jones, N. A.; Arnold, P. L., Low-Valent Uranium Iodides: Straightforward Solution Syntheses of UI_3 and UI_4 Etherates. *Inorg. Chem.* **2008,** *47*, 8577-8579.

26. Xie, Z.; Chiu, K.-Y.; Wu, B.; Mak, T. C. W., Autoionization of SmI_3 in Tetrahydrofuran. X-ray Crystal Structure of the Ionic Complex $[SmI_2(THF)_5][SmI_4(THF)_2]$. *Inorg. Chem.* **1996,** *35*, 5957-5958.

27. Niemeyer, M., trans-Diiodopentakis(tetrahydrofuran)ytterbium(III) tetraiodo-trans-bis(tetrahydrofuran)ytterbium(III). *Acta Crystallogr. E* **2001,** *57*, m363-m364.

28. Bradley, D. C.; Ghotra, J. S.; Hart, F. A., Low Co-ordination Numbers in Lanthanide and Actinide Compounds. Part I. The Preparation and Characterization of Tris{bis(trimethylsilyl)-amido}lanthanides. *J. Chem. Soc., Dalton Trans.* **1973**, 1021-1023.

29. Wooles, A. J.; Mills, D. P.; Lewis, W.; Blake, A. J.; Liddle, S. T., Lanthanide Tri-benzyl Complexes: Structural Variations and Useful Precursorsto Phosphorus-Stabilised Lanthanide Carbenes. *Dalton Trans.* **2010,** *39*, 500-510.

30. Evans, W. J.; Davis, B. L., Chemistry of Tris(pentamethylcyclopentadienyl) f-Element Complexes, $(C_5Me_5)_3M$. *Chem. Rev.* **2002,** *102*, 2119-2136.

31. Raymond, K. N.; Eigenbrot, J., C. W., Structural Criteria for the Mode of Bonding of Organoactinides and -Lanthanides and Related Compounds. *Acc. Chem. Res.* **1980,** *13*, 276-283.

32. Schwarzenbach, G.; Flaschka, H., *Complexometric Titrations*. Second ed.; United Kingdom, 1969.

33. Dolomanov, O. V.; Bourhis, L. J.; Gildea, R. J.; Howard, J. A. K.; Puschmann, H., OLEX2: A Complete Structure Solution, Refinement and Analysis Program. *J. Appl. Cryst.* **2009,** *42*, 339-341.

34. Sheldrick, G. M., SHELXT - Integrated Space-Group and Crystal-Structure Determination. *Acta Cryst.* **2015,** *A71*, 3-8.

35. Sheldrick, G. M., Crystal Structure Refinement with SHELXL. *Acta Cryst.* **2015,** *C71*, 3-8.

CHAPTER 3. SYNTHESIS AND METALATION OF AN ANIONIC PHENYLPYRIDINE LIGAND

3.1 Note on Collaboration

This chapter contains X-ray crystals structures that were solved by Dr. John Bacsa and Mr. Ningxin Jiang.

3.2 Background

The organic methodology community has embraced molecular photosensitizers and has developed a wide range of powerful methodologies dependent on photosensitizers to provide sufficient driving force to achieve reactive intermediates.[1-3] However, these methodologies are limited by the tool set available – $[Ru(bpy)_3]^{2+}$, $Ir(ppy)_3$, and their analogs (bpy = bipyridine and ppy = phenylpyridine) are the only photosensitizers employed. The scope of substrates is significantly limited by the redox potentials obtainable by the photoexcited states of these complexes. Here, two initial systems are proposed, based on successful transition metal ligands that are modified to match the redox chemistry and larger ionic radii of the lanthanides. The strategy is to employ ligands with orthogonal π^*-orbitals of appropriate energies to induce stabilization of the excited state from charge transfer or *f-d* absorptions of trivalent lanthanides. These excited states would not be directly correlated to the lanthanide ion excited state manifold and thus should experience an appreciable long lifetime.

Lanthanide bipyridine and phenanthroline complexes readily disassociate in solution.[4] In the case of actinide complexes, appropriate substitution on these ligand sets is essential to prevent ground state reduction of the ligand. The strategy then is to employ ligands with orthogonal π^*-orbitals of appropriate energies to induce stabilization of the excited state from charge transfer or *f-d* absorptions of trivalent lanthanides. These excited states would not be directly correlated to the lanthanide ion excited state manifold and thus should experience an appreciable long lifetime. Lanthanide analogs of $[Ru(bpy)_3]^{2+}$ and $Ir(ppy)_3$ photosensitizers can be prepared by employing *para*-alkyl groups on a cyclometalated phenylpyridine analog (Figure 3.1). This architecture prevents the reduced ligands in the photoexcited state from undergoing unproductive radical coupling reactions and the anionic cyclometalate disfavors photodissociation. It is possible to use this strategy to produce long-lived excited states. Using ligands with orthogonal π^* orbitals with the appropriate energy, it may be possible to stabilize the quartet state of the charge transfer transition or *f-d* absorptions of trivalent lanthanides and actinides.

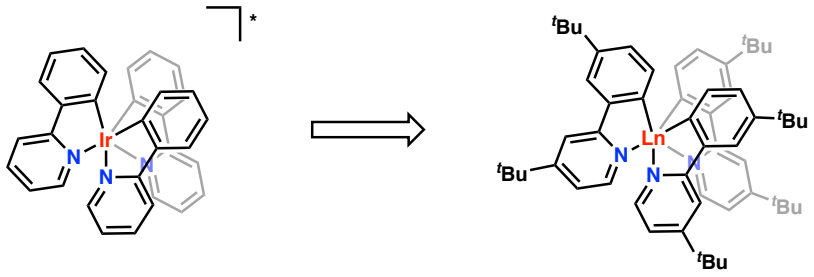

[Ir(ppy)]* Target analogous lanthanide complex.

Figure 3.1. Lanthanide analog of an excited-state transition-metal photosensitizer.

Polypyridyl adducts of lanthanide and actinide complexes have been well studied to understand the nature of a charge-transfer ground state. These studies have mainly focused on cerium, samarium, and ytterbium metallocenes to probe the electronic and magnetic behavior of these molecular species due to the charge-transfer ground state.[4-9] Here, analogous complexes using a phenylpyridine ligand will be synthesized to study the effects of changing the charge of the ligand and substitutions on the ligand.

The polypyridyl ligand utilized is a LX-type donor, where L is a two-electron donor and X is a one-electron donor. The phenylpyridine contains a bromide which can undergo lithium-halogen exchange to afford a transmetalation reagent to undergo salt metathesis with a lanthanide halide starting material. The synthesis of the ligand will be described later on. Pentamethylcyclopentadienyl (Cp*) chemistry has been well studied in the lanthanides (and actinides).[10-12] Utilizing the Cp* ligand as a starting point, the photochemistry of the lanthanides using the phenylpyridine ligand can be studied. Complexes of the type $Cp^*_2Ln(L)$, where Ln = lanthanide and L = polypyridyl (bipyridine, phenanthroline, terpyridine, etc.) have

been previously studied. To undergo salt metathesis, lanthanide starting materials of the type $Cp^*_2LnX(sol)$, where X = halide and sol = solvent, must be synthesized. Lanthanide tribromides and trichlorides have been used to yield these types of starting materials but involve labor-intensive dehydration of their hydrated forms. More recently, solvated lanthanide triiodides have been utilized as convenient lanthanide starting materials, including efforts from our group (Chapter 2). This chapter will describe the synthesis of the ligand and of a complex bearing the formula $Cp^*_2Ln(L)$ to demonstrate first-principles of metalation using the ligand.

3.3 Results and Discussion

3.3.1 Synthesis of ppy

This phenylpyridine analog of the conventional 2-phenylpyridine ligand is synthesized in three steps. First, a Grignard reagent is prepared from 3-*tert*-butylbromobenzene and the Grignard undergoes electrophilic borylation to give the corresponding arylboronic acid (Scheme 3.1).[13-14] Maiti's iron-mediated cross-coupling is then utilized to couple 3-*tert*-butylboronic acid to 4-*tert*-butylpyridine yielding phenylpyridine (ppy), **1**.[15] Baran has reported on the direction C-H arylation of electron-deficient hetereocycles with arylboronic acids using catalytic silver(I) nitrate and persulfate as a co-oxidant.[16] However, this methodology resulted in lower yields (32% vs. 46% for the Maiti procedure) for the same substrates. The bromination of the 2-position of the phenyl ring allows for the compound to serve as a pre-ligand for metalation reactions. Therefore, Sanford's

nitrogen-directed C-H bromination is used to give the bromophenylpyridine compound (Br-ppy), **2**.[17]

Scheme 3.1. Synthesis of the phenylpyridine ligand.

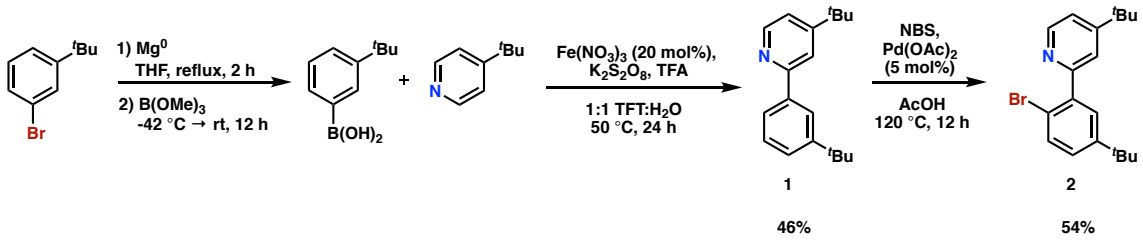

3.3.2 Synthesis and X-ray Crystal Structure of Li-ppy

The lithium salt of bromophenylpyridine compound, **2**, can be synthesized through lithium-halogen exchange with *n*-butyllithium in diethyl ether at -35 °C (Scheme 3.2). Concentration of the solvent *in vacuo* and allowing the solution to maintain temperature in a -35 °C freezer overnight affords the lithium salt, **2-Li**, in good yield, as yellow plates.

Scheme 3.2. Synthesis of Li-ppy.

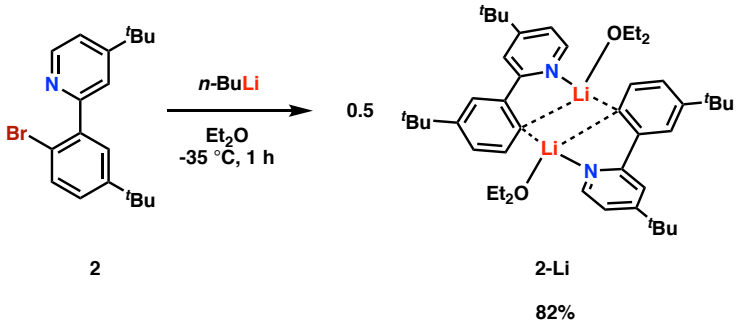

Single solvent crystallization of the product from the reaction mixture affords yellow crystals suitable for single crystal X-ray diffraction. $[(ppy)Li(OEt_2)]_2$ forms a dimeric structure similar to that observed for $[LiPh(TMEDA)]_2$ (Figure 3.2).[18] Here, the lithium ions bridge the aryl groups and interact with the *ipso* carbons of the aryl rings to afford a nearly planar Li_2C_2 core. The lithium ions are also supported by the nitrogen on the pyridine ring and the oxygen atom on the ethereal solvent to give the four-coordinate metal center.

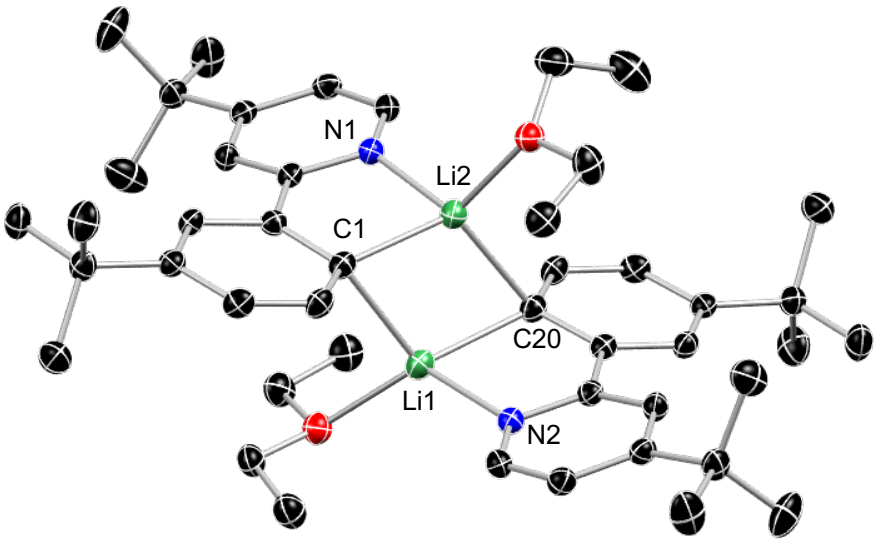

Figure 3.2. Molecular structure of **2-Li** with thermal ellipsoids shown at 50% probability. H atoms are omitted for clarity.

3.3.3 Synthesis and Characterization of $Cp^*_2Sm(ppy)$

The original synthesis of $Cp^*_2Sm(ppy)$, **3-Sm**, involved the reaction between divalent $Cp^*_2Sm(THF)_2$ and Li-ppy that was generated *in situ*. X-ray quality crystals were grown out of a concentrated solution of pentane at -35 °C and yielded $Cp^*_2Sm(ppy)$, **3-Sm**, in a roughly 25% yield (Figure 3.3).

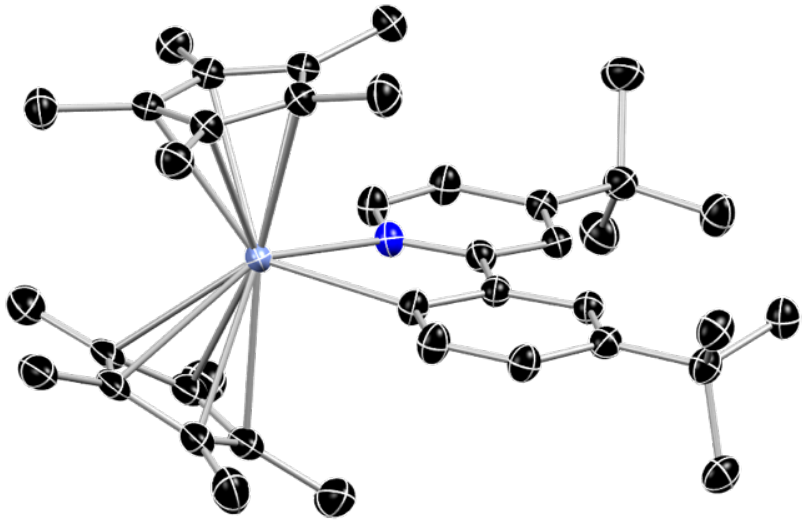

Figure 3.3. Molecular structure of **3-Sm** with thermal ellipsoids shown at 50% probability. H atoms are omitted for clarity.

The reaction between divalent $Cp^*_2Sm(THF)_2$ and **2-Li** should result in a divalent Sm metal in the product. However, the reaction product was a dark blue-green oil and the color of the crystals were yellow. This yellow color is indicative of a trivalent samarium complex. A Teflon stir bar was used in the reaction vessel and could have been reduced by the intended divalent Sm anionic complex or decomposed to from a more stable and neutral trivalent complex.

Analysis of the bond lengths and angles in the crystal structure will aid in confirming a Sm(3+) complex. The average Sm-Cp^*_{cent} distance is 2.034 Å and the average Sm-C_{ring} distance is 2.722(6) Å, and is within the range of 2.68-2.77 Å for known $Cp^*_2Sm(3+)$ complexes, and outside the range of 2.79-2.86 Å for $Cp^*_2Sm(2+)$ complexes. The Sm-C_{ring} distance compares well to the reported distance of 2.724(3) Å for $Cp^*_2Sm(bpy)$.[9] Additionally, the Cp^*_{cent}-Sm-Cp^*_{cent} angle of 141.6° also compares well to that of the $Cp^*_2Sm(bpy)$ complex with an angle of

137.9°. The average Sm-N distance in $Cp^*_2Sm(bpy)$ was reported to be 2.431(2) Å, which is also comparable to the Sm-N distance in **3-Sm** of 2.482(5) Å and Sm-C_{phenyl} distance of 2.459 Å.[9] The most distinctive parameter for the characterization of the redox-active ppy ligand is the C-C bond distance between the carbon atoms connecting the pyridine to the phenyl moiety to access the extent of ligand reduction (Figure 3.4). In the case of complex **3-Sm**, this bond distance was determined to be 1.488(8) Å. This distance can be compared with Ln complexes containing monoreduced $bpy^{\bullet-}$ radicals [1.429(4)-1.445(17) Å] and neutral bpy [1.490(3) Å].[19] The C-C bond distance is longer than that of monoreduced $bpy^{\bullet-}$ radicals and is similar to that of neutral bpy. Hence, the XRD data support a Sm(3+) and neutral ppy formulation.

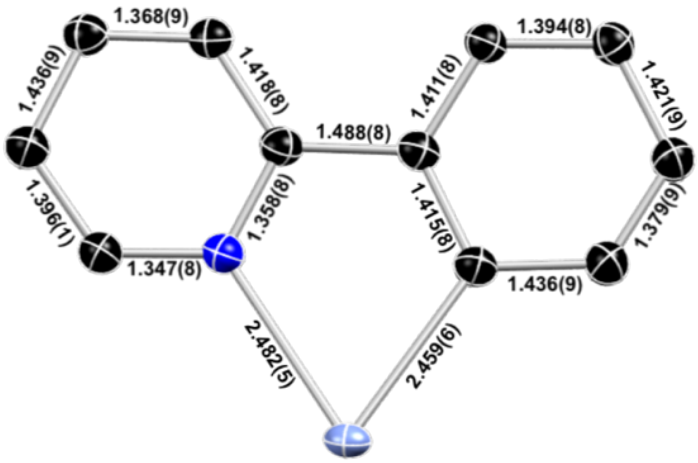

Figure 3.4. Samarium-phenylpyridine core structure with the corresponding bond distances in Å of complex **3-Sm**.

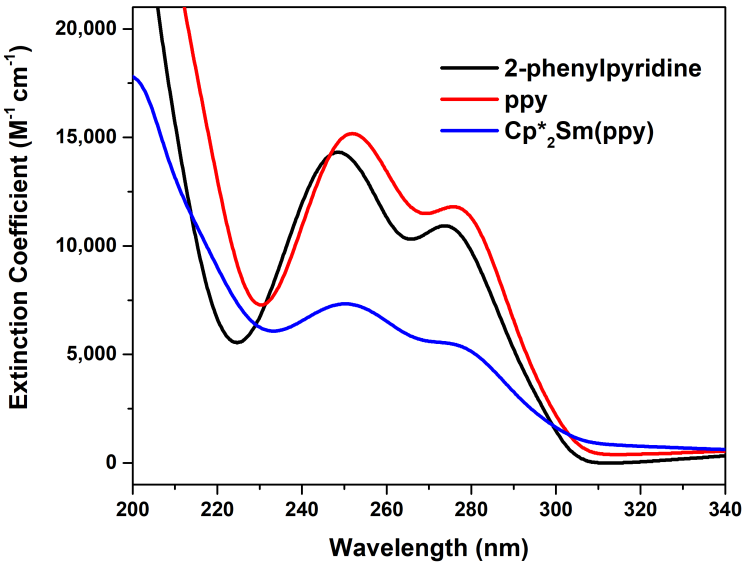

Figure 3.5. Electronic spectral data for 2-phenylpyridine, **1** (ppy), and **3-Sm** [$Cp^*_2Sm(ppy)$] in hexanes.

UV-vis absorption spectra were obtained for 2-phenypyridine, ppy (**2**), and $Cp^*_2Sm(ppy)$ (**3-Sm**) in hexanes solution. The spectra are illustrated in Figure 3.5. For comparison, the UV-vis-NIR spectra of $bpy^{\bullet-}$ radical anions can be used. The characteristic features of this radical anion are from the presence of an unpaired electron in a π^* orbital. These features consist of (i) a strong-intensity band at ~400 nm, (ii) a medium-intensity band at ~500 nm, and (iii) a weak band in the NIR at ~900 nm.[19] However, the UV-vis spectrum of **3-Sm** does not contain lower energy absorptions past 300 nm. In comparing the spectrum of **3-Sm** with the free ligand **2**, the two spectra are nearly superimposable and display similar features. Thus, the UV-vis spectra support that complex **3-Sm** contains a neutral ppy ligand. It is also noteworthy that the *para* substitution results in a bathochromic shift of roughly

4 nm for both ligand-centered ($\pi \rightarrow \pi^*$) transitions. Additionally, the extinction coefficient of **3-Sm** is roughly half that of free ligand.

After the synthesis of **3-Sm**, the lithium salt, **2-Li**, was crystallized and could be used in metalation reactions. The lithium salt can undergo salt metathesis with a lanthanide halide starting material. Here, one equivalent of **2-Li** can be mixed with $Cp^*_2Sm(I)(THF)$ in diethyl ether at -35 °C for 24 h to yield $Cp^*_2Sm(ppy)$, as shown in Scheme 3.3.

Scheme 3.3. Synthesis of $Cp^*_2Sm(ppy)$.

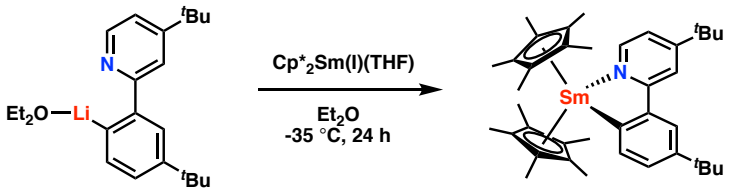

2-Li **3-Sm** **77%**

The reaction between trivalent $Cp^*_2Sm(I)(THF)$ and Li-ppy (**2-Li**) yields the corresponding salt metathesis product, $Cp^*_2Sm(ppy)$, **3-Sm**. A concentrated solution of **3-Sm** in pentane at -35 °C gives X-ray quality crystals whose unit cell paramters match that of the original reaction between $Cp^*_2Sm(THF)_2$ and Li-ppy.

3.4 Conclusion

A new phenylpyridine analog was synthesized in an overall 25% yield over three steps. This ligand can undergo lithium-halogen exchange to generate an overall anionic lithium salt complex that can be isolated and used to complex onto

lanthanide ions. In the case shown here, the lithium salt was ligated to generate the $Cp^*_2Sm(ppy)$ complex, in which its electronic properties can be further explored to investigate the photochemistry and photophysics of trivalent lanthanides.

3.5 Experimental

3.5.1 General Considerations

Unless otherwise noted, all reagents were obtained from commercial suppliers and the syntheses and manipulations were conducted under argon with exclusion of oxygen and water using Schlenk techniques or in an inert atmosphere box (Vigor) under a dinitrogen (<0.1 ppm O_2/H_2O) atmosphere. The glovebox is equipped with two -35 °C freezers. All glassware and cannulae were stored in an oven over-night (>8 h) at a temperature of ca. 160 °C. Celite and molecular sieves were dried under vacuum at a temperature >250 °C for a minimum of 24 h. C_6D_6 was stored over 3 Å molecular sieves and then vacuum-transferred from purple sodium/benzophenone prior to use. Pentane, *n*-hexane, diethyl ether, toluene, and tetrahydrofuran were purged with UHP-grade argon (Airgas) and passed through columns containing Q-5 and molecular sieves in a solvent purification system (JC Meyer Solvent Systems). All solvents in the glovebox were stored in bottles over 3 Å molecular sieves. Trimethyl borate was dried over sodium, then distilled and degassed. Pentamethylcyclopentadiene was freeze-pump-thawed three times and then stored over 3 Å molecular sieves. $SmI_2(THF)_2$,[20] $(Cp^*)_2Sm(THF)_2$[21] and $(Cp^*)_2Sm(I)(THF)$[22] were all synthesized according to reported procedures. NMR

spectra were obtained on a Bruker Advance III 400 MHz or Bruker Advance III HD 500 MHz spectrometer at 298 K, unless otherwise noted. ^{1}H and ^{13}C NMR chemical shifts are reported in δ, parts per million. ^{1}H and ^{13}C NMR are references to the residual proton and carbon resonances of the solvent, respectively.[23] Peak position is listed, followed by peak multiplicity, integration value, and proton assignment, where applicable. Multiplicity and shape are indicated by one or more of the following abbreviations: s (singlet); d (doublet); t (triplet); q (quartet); dd (doublet of doublets); td (triplet of doublets); m (multiplet); br (broad). UV-vis-NIR spectra were obtained on a Schimadzu UV-3101PC. FT-IR spectra were obtained on a Bruker Alpha-P FT-IR with an ATR platinum diamond reflector accessory. Elemental analyses were determined at Robertson Microlit Laboratories (Ledgewood, NJ). X-ray structural determinations were performed at the Georgia Institute of Technology on a Bruker D8 Venture diffractometer.

3.5.2 Synthetic Procedures

3.5.2.1 4-*tert*-butyl-2-(3-*tert*-butyl)phenylpyridine (**1**)

To a three-neck 250-mL round-bottom flask was added magnesium turnings (1.25 g, 51.4 mmol, 1.1 eq) and 3-*tert*-butylbromobenzene (2.0 g, 9.4 mmol, 0.2 eq). THF (10 mL) was added via addition funnel, to which a crystal of iodine was also added. Then, the remaining 3-*tert*-butylbromobenzene (8.0 g, 37.5 mmol, 0.8 eq) was slowly added via addition funnel. The solution was heated to reflux for 2 h under argon. The Gringard was cooled to rt and then diluted with THF (to double its volume). The solution was slowly transferred via cannula over 20 min

to a cooled solution (-40 °C) of trimethyl borate (9.0 mL, 93.8 mmol, 2.0 eq) dissolved in THF (100 mL), forming a white precipitate. *Note:* If the Grignard became too viscous, THF was added to the solution. The mixture was allowed to stir and warm to rt overnight. After quenching with 1 M HCl to pH 2, the mixture was extracted with dichloromethane (2 x 60 mL) and the organic layer was dried over sodium sulfate and was dried *in vacuo*. The solid was recrystallized in hexanes with a small amount of ethyl acetate. Cooling the solution to rt crashes out an off-white solid, which was then filtered from the solution. The solution was then further cooled to afford the product as a white solid (4.20 g, 50%). The crude product can be used in the next step without further purification. To an oven-dried 350 mL Schlenk flask with a Teflon tap was added potassium persulfate (17.27 g, 63.90 mmol), iron nitrate nonahydrate (1.290 g, 20 mol%), 4-*tert*-butylpyridine (2.34 mL, 16.0 mmol, 1.0 eq), and trifluoroacetic acid (2.20 mL, 19.2 mmol, 1.2 eq). Then, α,α,α-trifluorotoluene (62 mL) and distilled water (62 mL) were added. The vessel was sealed and stirred for 10 min at rt. Then, 3-*tert*-butylboronic acid (8.530 g, 47.9 mmol, 3.0 eq) was added to the mixture. The reaction mixture again sealed and was vigorously stirred and heated at 50 °C for 24 h. The reaction mixture was cooled to rt and extracted with ethyl acetate (3 x 60 mL) and washed with saturated sodium bicarbonate solution (1 x 60 mL). The organic layers were combined and dried over sodium sulfate. The resulting product was concentrated *in vacuo* and purified by column chromatography on neutral alumina (R_f = 0.61 in 90% hexanes/10% EtOAc) to afford the product as a golden yellow solid, which can be further recrystallized in hexanes to give a white solid (1.952 g, 46%). ^{1}H NMR (500

MHz, $CDCl_3$, δ): 8.61 (dd, *J* = 5.3, 0.6 Hz, 1H, Ar-*H*), 8.02 (t, *J* = 1.7 Hz, 1H, Ar-*H*), 7.71 (dt, *J* = 7.7, 1.7 Hz, 1H, Ar-*H*), 7.68 (dd, *J* = 1.9, 0.6 Hz, 1H, Ar-*H*), 7.46 (ddd, *J* = 7.7, 1.9, 1.3 Hz, 1H, Ar-*H*), 7.41 (t, *J* = 7.7 Hz, 1H, Ar-*H*), 7.23 (dd, *J* = 5.3, 1.9 Hz, 1H, Ar-*H*), 1.40 (s, 9H, $C(CH_3)_3$), 1.37 (s, 9H, $C(CH_3)_3$). ^{1}H NMR (500 MHz, C_6D_6, δ): 8.65 (dd, *J* = 5.2, 0.7 Hz, 1H, Ar-*H*), 8.60 (t, *J* = 1.7 Hz, 1H, Ar-*H*), 7.97 (dt, *J* = 7.8, 1.3 Hz, 1H, Ar-*H*), 7.74 (dd, *J* = 1.8, 0.7 Hz, 1H, Ar-*H*), 7.37 (ddd, *J* = 7.8, 1.8, 1.3 Hz, 1H, Ar-*H*), 7.33 (dd, *J* = 1.8, 0.7 Hz, 1H, Ar-*H*), 6.84 (dd, *J* = 5.2, 1.7 Hz, 1H, Ar-*H*), 1.32 (s, 9H, $C(CH_3)_3$), 1.10 (s, 9H, $C(CH_3)_3$). ^{13}C NMR (126 MHz, $CDCl_3$, δ): 160.71 (aryl-*C*), 158.37 (aryl-*C*), 151.73 (aryl-*C*), 149.66 (aryl-*C*), 140.07 (aryl-*C*), 128.48 (aryl-*C*), 125.98 (aryl-*C*), 124.42 (aryl-*C*), 124.29 (aryl-*C*), 119.30 (aryl-*C*), 118.17 (aryl-*C*), 35.02 ($C(CH_3)_3$), 34.99 ($C(CH_3)_3$), 31.57 ($C(CH_3)_3$), 30.76 ($C(CH_3)_3$). Anal. Calcd for $C_{19}H_{25}N$: C, 85.34; H, 9.42; N, 5.24. Found: C, 85.21; H, 9.07; N 5.27.

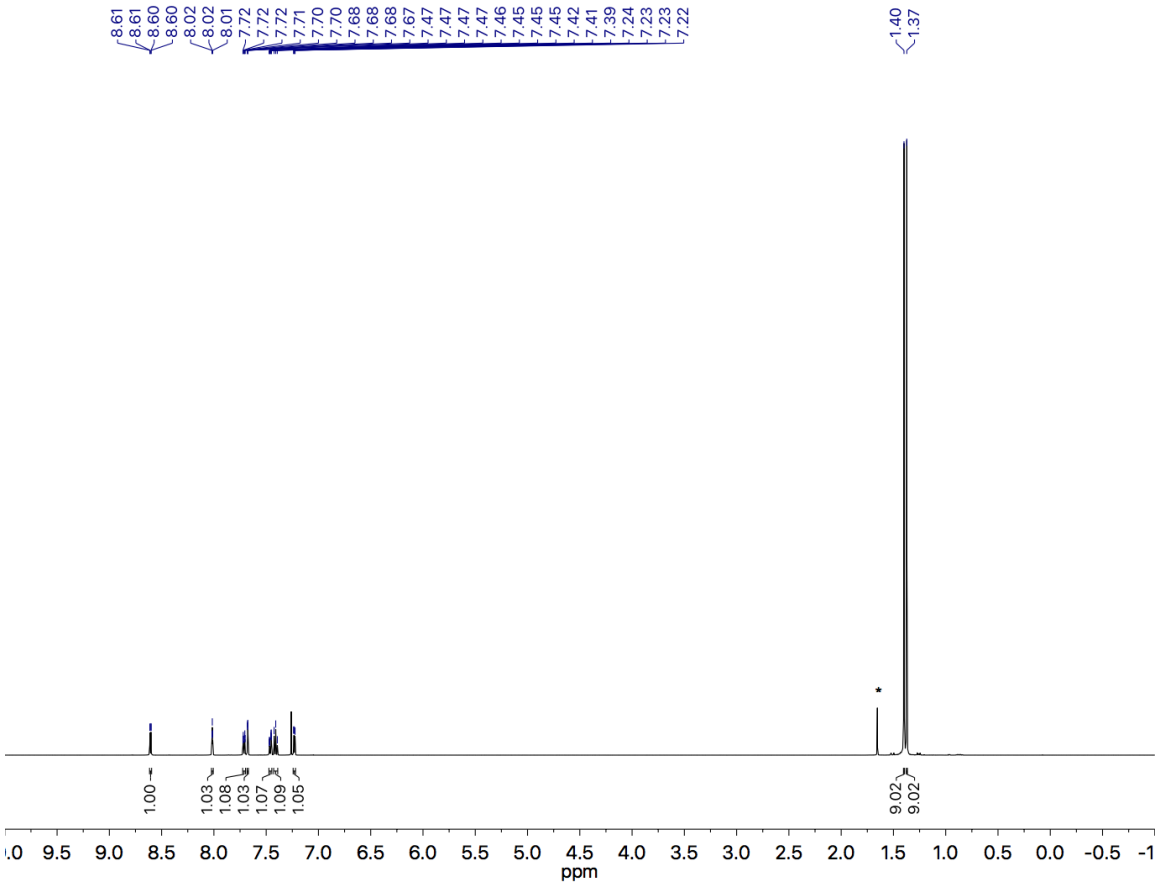

Figure 3.6. ^{1}H NMR (500 MHz, $CDCl_3$) of ppy (**1**). Residual water is noted by *.

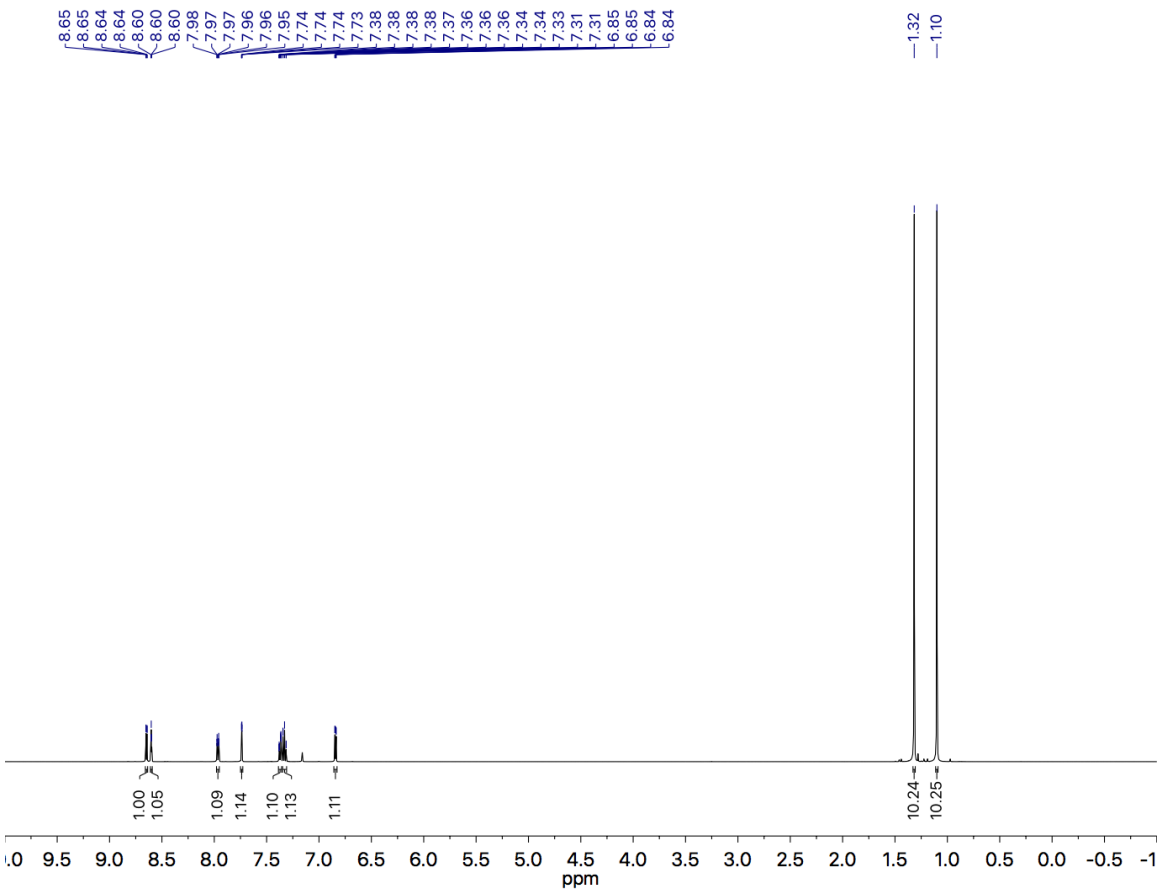

Figure 3.7. ^{1}H NMR (500 MHz, C_6D_6) of ppy (**1**).

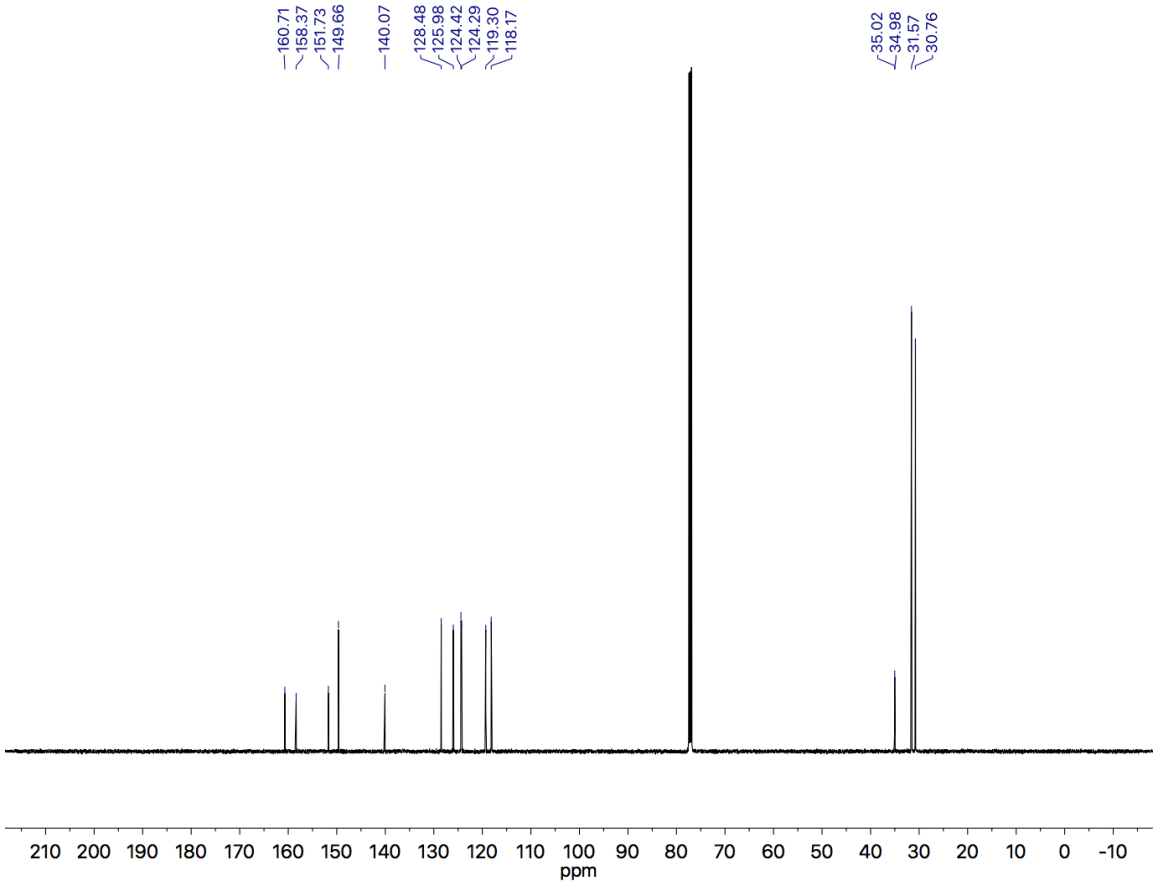

Figure 3.8. ^{13}C NMR (126 MHz, $CDCl_3$) of ppy (**1**).

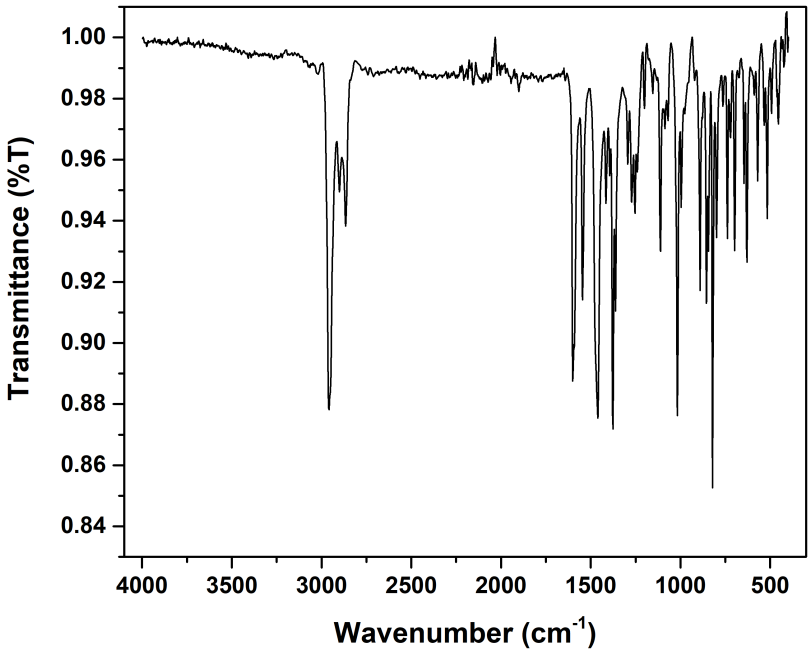

Figure 3.9. ATR-FTIR spectrum of ppy (**1**).

3.5.2.2 2-(2-bromo-5-*tert*-butylphenyl)-4-*tert*-butylpyridine (**2**)

To a 50 mL Schlenk flask with a Teflon tap was added a solution of **1** (2.14 g, 8.00 mmol, 1.0 eq), *N*-bromosuccinimide (1.71 g, 9.60 mmol, 1.2 eq), and palladium(II) acetate (0.090 g, 5 mol%) in acetic acid (35 mL). The vessel was sealed, and the mixture was vigorously stirred and heated at 120 °C for 12 h. The solvent was removed *in vacuo* and the residue was purified by column chromatography on silica gel (R_f = 0.32 in 10% EtOAc in hexanes) to afford the golden yellow oil. Volatiles were removed *in vacuo* on a Schlenk line to 3.0 mTorr before placing the oil in a -80 °C freezer overnight. Allowing the oil to warm up to rt yields a pale yellow solid. The product was then sublimed (70 °C, 3.0 mTorr) to

yield a white solid (1.6072 g, 58%). ^{1}H NMR (500 MHz, $CDCl_3$, δ): 8.61 (dd, *J* = 5.3, 0.7 Hz, 1H, Ar-*H*), 7.61 (dd, *J* = 2.2, 0.7 Hz, 1H, Ar-*H*), 7.58 (d, *J* = 5.3 Hz, 1H, Ar-*H*), 7.56 (d, *J* = 2.2 Hz, 1H, Ar-*H*), 7.28 (dd, *J* = 3.4, 2.2 Hz, 1H, Ar-*H*), 7.27 (dd, *J* = 3.4, 2.2 Hz 1H, Ar-*H*), 1.36 (s, 9H, $C(CH_3)_3$), 1.34 (s, 9H, $C(CH_3)_3$). ^{1}H NMR (500 MHz, C_6D_6, δ): 8.63 (dd, *J* = 5.3, 0.8 Hz, 1H, Ar-*H*), 7.96 (d, *J* = 2.6 Hz, 1H, Ar-*H*), 7.77 (dd, *J* = 1.9, 0.8 Hz, 1H, Ar-*H*), 7.53 (d, *J* = 8.4 Hz, 1H, Ar-*H*), 6.95 (dd, *J* = 8.4, 2.6 Hz, 1H, Ar-*H*), 6.86 (dd, *J* = 5.3, 1.9 Hz, 1H, Ar-*H*), 1.14 (s, 9H, $C(CH_3)_3$), 1.11 (s, 9H, $C(CH_3)_3$). ^{13}C NMR (126 MHz, $CDCl_3$, δ): 159.72 (aryl-*C*), 158.56 (aryl-*C*), 150.86 (aryl-*C*), 149.40 (aryl-*C*), 141.18 (aryl-*C*), 132.94 (aryl-*C*), 128.63 (aryl-*C*), 127.16 (aryl-*C*), 122.54 (aryl-*C*), 119.47 (aryl-*C*), 118.83 (aryl-*C*), 34.98 ($C(CH_3)_3$), 34.82 ($C(CH_3)_3$), 31.38 ($C(CH_3)_3$), 30.66 ($C(CH_3)_3$). Anal. Calcd for $C_{19}H_{24}BrN$: C, 65.90; H, 6.99; N, 4.04. Found: C, 65.57; H, 6.87; N 3.97.

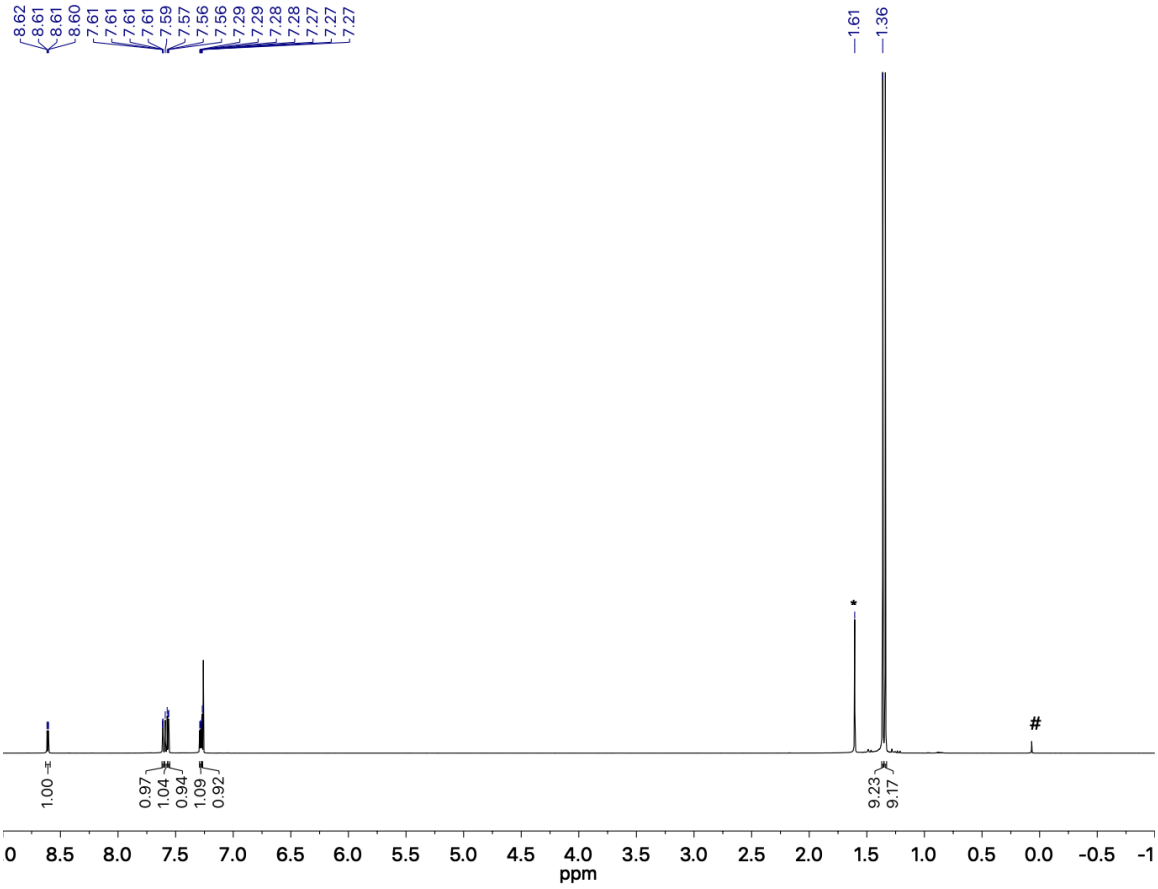

Figure 3.10. ^{1}H NMR (500 MHz, $CDCl_3$) of Br-ppy (**2**). Residual silicone grease, water, are noted by # and *, respectively.

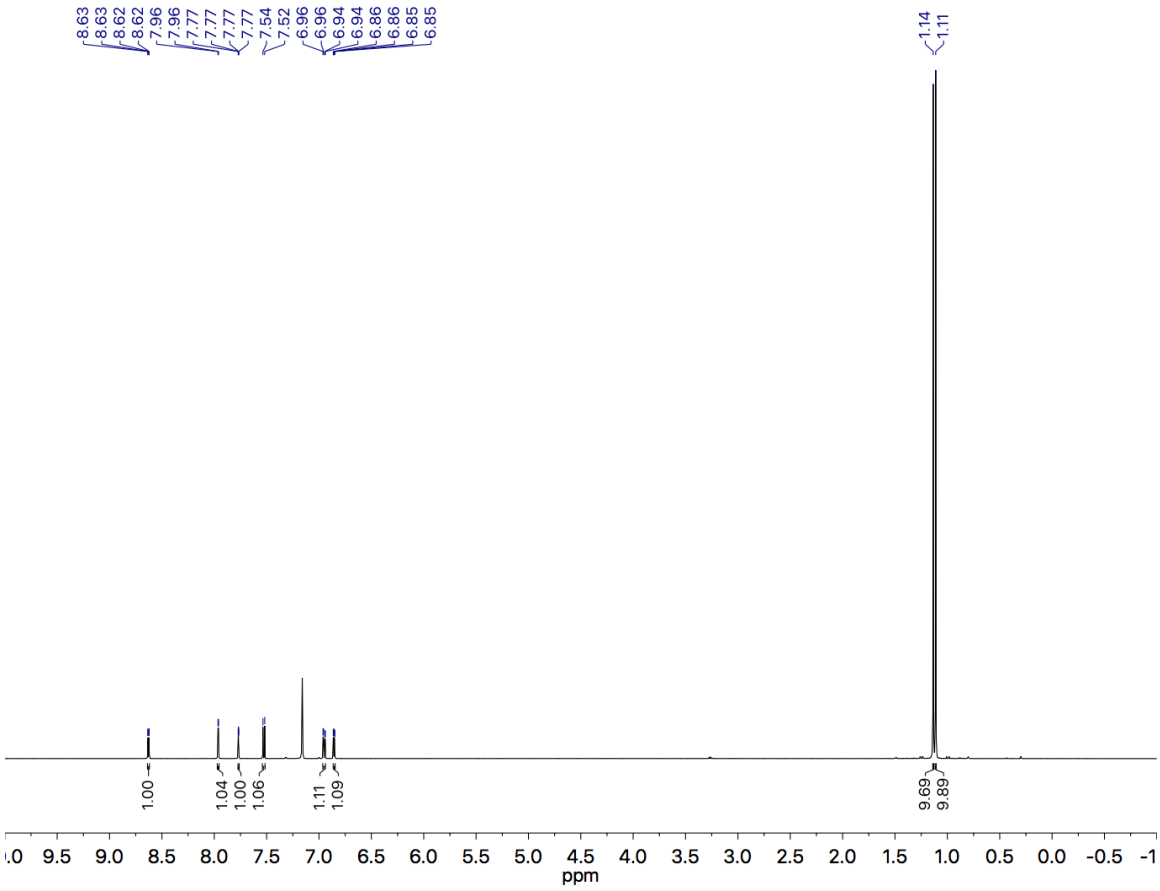

Figure 3.11. ^{1}H NMR (500 MHz, C_6D_6) of Br-ppy (**2**).

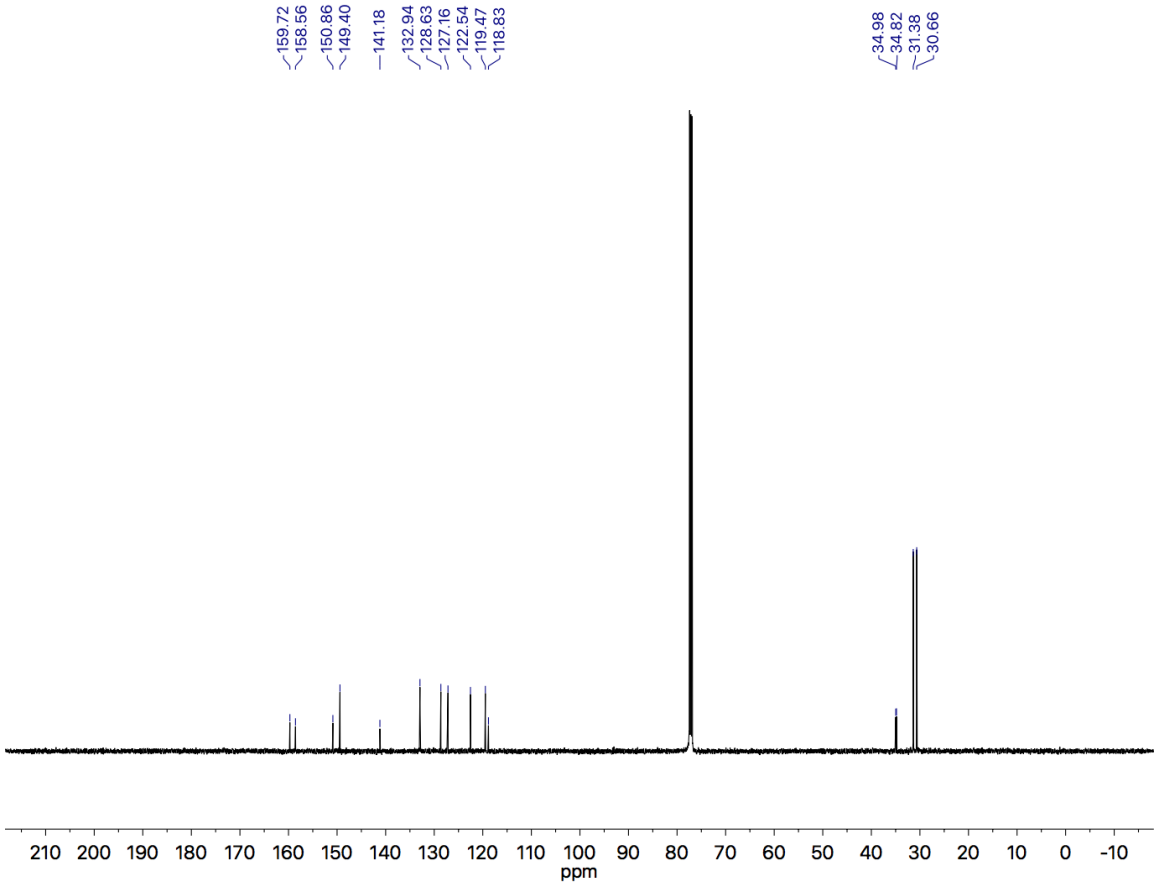

Figure 3.12. ^{13}C NMR (126 MHz, $CDCl_3$) of Br-ppy (**2**).

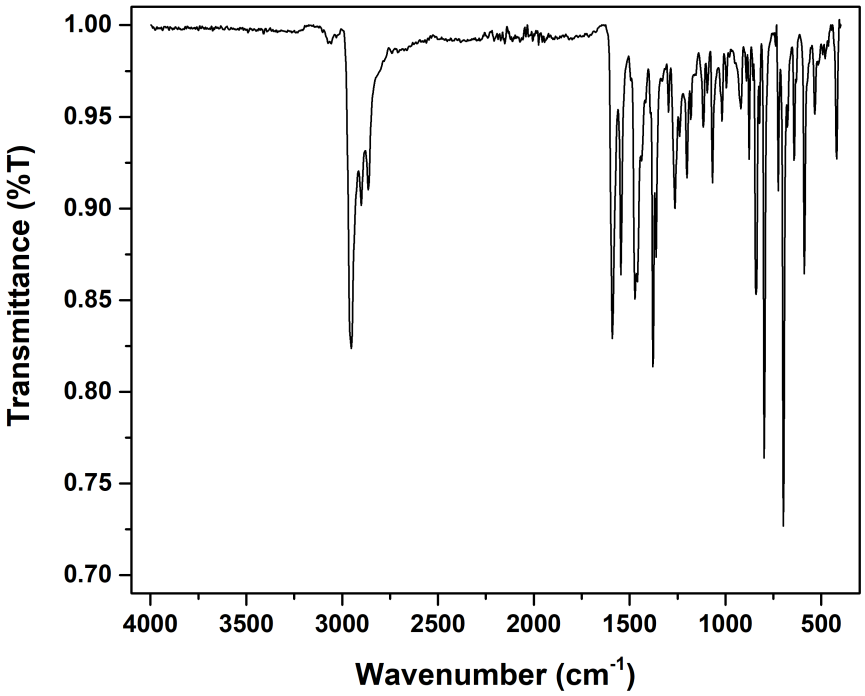

Figure 3.13. ATR-FTIR spectrum of Br-ppy (**2**).

3.5.2.3 Li-ppy (**2-Li**)

In a 20 mL scintillation vial, **2** (0.588 g, 1.70 mmol, 1.0 eq), was dissolved diethyl ether (5 mL). The solution was then chilled in a -35 °C freezer for 20 min before *n*-BuLi (0.77 mL, 1.70 mmol, 1.0 eq, 2.2 M in hexanes) was added dropwise to the solution while remaining in the freezer. The solution was swirled for 30 s every 10 min for 1 h. The yellow solution was then concentrated *in vacuo* before allowing the product to crystallize overnight, yielding yellow crystals (0.380 g, 82%). Due to the thermal instability of this complex, elemental analysis and NMR data were unable to be obtained.

3.5.2.4 $Cp^*_2Sm(ppy)$ (**3-Sm**)

In a 20 mL scintillation vial, Cp*Sm(I)(THF) (0.101 g, 0.156 mmol, 1.0 eq) was dissolved in diethyl ether (2 mL). The solution was then chilled in a -35 °C freezer for 20 min before a chilled (-35 °C) solution of **2-Li** (0.054 g, 0.15 mmol, 1.0 eq) in diethyl ether (2 mL) was added dropwise to the solution while remaining in the freezer. The dark orange solution was swirled for 30 s every hour for 6 h with the solution turning yellow. The solution was left in the freezer for an additional 18 h before the yellow solution was concentrated *in vacuo* before allowing the product to crystalize overnight, yielding yellow crystals (0.087 g, 77%). ^{1}H NMR (400 MHz, C_6D_6, δ): 10.00 (d, *J* = 1.0 Hz, 1 H, Ar-*H*), 9.29 (d, *J* = 1.0 Hz, 1H, Ar-*H*), 6.49 (s, 1H, Ar-*H*), 2.56 (s, 1H, Ar-*H*), 1.99 (s, 9H, $C(CH_3)_3$), 1.37 (s, 30H, Cp*-*H*), 0.65 (s, 9H, $C(CH_3)_3$), -3.08 (br, 1H, Ar-*H*), -14.19 (br, 1H, Ar-*H*).

3.5.2.5 $Cp^*_2Sm(ppy)$ via $Cp^*_2Sm(THF)_2$

To a 50 mL Schlenk flask equipped with a stir bar was added a solution of **2** (0.155 g, 0.448 mmol, 1.0 eq) in THF (8 mL). The Schlenk flask was chilled to -78 °C and *n*-BuLi (0.16 mL, 0.45 mmol, 1.0 eq, 2.8 M in hexanes) was slowly added dropwise via syringe during which the light-yellow solution turned a deeper yellow color. The temperature was maintained, and the solution was allowed to stir for 6 h. The solution was then cannula transferred to a chilled (-78 °C) 100 mL Schlenk flask equipped with a stir bar and charged with $Cp^*_2Sm(THF)_2$ (0.266 g, 0.448 mmol, 1.0 eq) in THF (8 mL). The solution was slowly warmed up to room temperature over the course of 4 h and was then allowed to stir for an additional 12 h. The volatiles were evaporated *in vacuo*, triturated with pentane (3 x 2 mL),

taken up with pentane, and the product was filtered over Celite in fine porosity, sintered glass frit. The filtrate was evaporated *in vacuo* yielding a dark blue-green residue. Mass recovery: 0.279 g (86%).

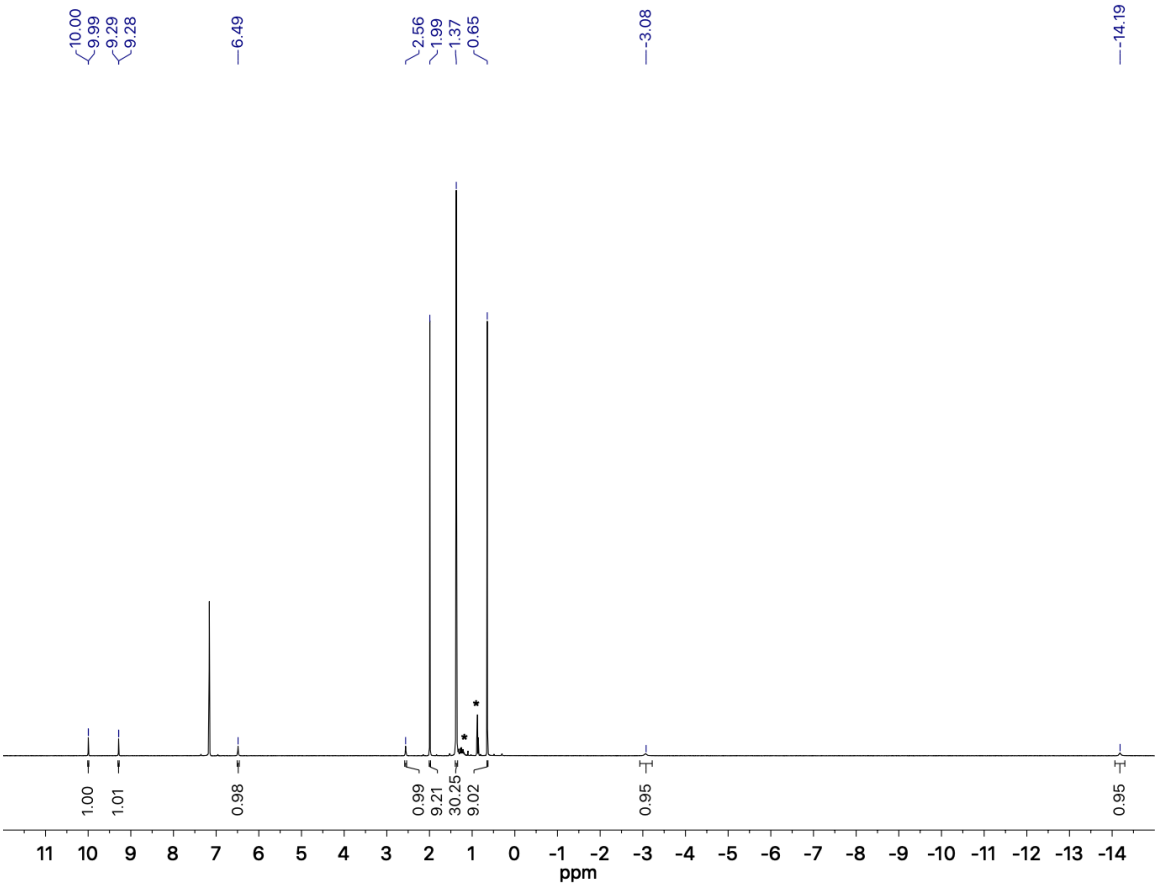

Figure 3.14. ^{1}H NMR (400 MHz, C_6D_6) of $Cp^*_2Sm(ppy)$ (**3-Sm**). Residual pentane is noted by *.

3.5.3 X-ray Diffraction Data

3.5.3.1 Li-ppy (**2-Li**)

Experimental. Single yellow, prism-shaped crystals of Li-ppy were crystallized from a concentrated solution in pentane at -35 °C. A suitable crystal

0.206×0.276×0.332 mm^2 was selected and mounted on a loop with paratone oil on a Bruker D8 Venture diffractometer with MO Kα radiation and PHOTON II detector. The crystal was kept at 100.01 K during data collection. Using Olex2,[24] the structure was solved with ShelXT[25] structure solution program using Intrinsic Phasing and refined with ShelXL[26] refinement package using Least Squares Minimization.

Crystal Data. $C_{184}H_{272}Li_8N_8O_8$ (M = 2779.60 g/mol): monoclinic, space group $P2_1/c$ (no. 14), a = 20.617(4) Å, b = 11.25560(19) Å, c = 18.923(3) Å, β = 97.974(6)°, V = 4348.9(13) $Å^3$, Z = 1, T = 100.01 K, μ(Mo Kα) = 0.063 mm^{-1}, *Dcalc* = 1.061 g/cm^3, 62175 reflections measured (4.346° ≤ 2θ ≤ 56.562°), 10782 unique (R_{int} = 0.0796, R_{sigma} = 0.0562) which were used in all calculations. The final R_1 was 0.0534 (I > 2σ(I)) and wR_2 was 0.1430 (all data).

3.5.3.2 $Cp^*_2Sm(ppy)$ (**3-Sm**)

Experimental. Single yellow, plate-shaped crystals of $Cp^*_2Sm(ppy)$ were crystallized from a concentrated solution in pentane at -35 °C. A suitable crystal 0.154×0.464×0.656 mm^2 was selected and mounted on a loop with paratone oil on a Bruker D8 Venture diffractometer with Mo Kα radiation and PHOTON II detector. The crystal was kept at 100(2) K during data collection. Using Olex2,[24] the structure was solved with ShelXT[25] structure solution program using Intrinsic Phasing and refined with ShelXL[26] refinement package using Least Squares Minimization.

Crystal Data. $C_{38}H_{54}N_2Sm$ (M = 689.18 g/mol): orthorhombic, space group Pbca (no. 61), a = 17.474(5) Å, b = 18.571(5) Å, c = 24.759(8) Å, V =

8035(4) $Å^3$, Z = 8, T = 100(2) K, μ(Mo Kα) = 1.485 mm^{-1}, *Dcalc* = 1.139 g/cm^3, 128869 reflections measured (4.59° ≤ 2θ ≤ 72.864°), 17682 unique (R_{int} = 0.1020, R_{sigma} = 0.0690) which were used in all calculations. The final R_1 was 0.1156 (I > 2σ(I)) and wR_2 was 0.3176 (all data).

3.6 References

1. Nicewicz, D. A.; MacMillan, D. W. C., Merging Photoredox Catalysis with Organocatalysis: The Direct Asymmetric Alkylation of Aldehydes. *Science* **2008,** *322*, 77-80.

2. Schultz, D. M.; Yoon, T. P., Solar Synthesis: Prospects in Visible Light Photocatalysis. *Science* **2014,** *343*, 985.

3. Choi, G. J.; Zhu, Q.; Miller, D. C.; Gu, C. J.; Knowles, R. R., Catalytic Alkylation of Remote C-H Bonds Enabled by Proton-Coupled Electron Transfer. *Nature* **2016,** *539*, 268-271.

4. Schultz, M.; Boncella, J. M.; Berg, D. J.; Tilley, T. D.; Andersen, R. A., Coordination of 2,2'-Bipyridyl and 1,10-Phenanthroline to Substituted Ytterbocenes: An Experimental Investigation of Spin Coupling in Lanthanide Complexes. *Organometallics* **2002,** *21*, 460-472.

5. Walter, M. D.; Booth, C. H.; Lukens, W. W.; Andersen, R. A., Cerocene Revisited: The Electronic Structure of and Interconversion Between $Ce_2(C_8H_8)_3$ and $Ce(C_8H_8)_2$. *Organometallics* **2009,** *28*, 698-707.

6. Berg, D. J.; Boncella, J. M.; Andersen, R. A., Preparation of Coordination Compounds of Cp^*_2Yb with Heterocyclic Nitrogen Bases: Examples of Antiferromagnetic Exchange Coupling across Bridging Ligands. *Organometallics* **2002,** *21*, 4622-4631.

7. Walter, M. D.; Berg, D. J.; Andersen, R. A., Coordination Complexes of Decamethylytterbocene with 4,4'-Disubstituted Bipyridines: An Experimental Study of Spin Coupling in Lanthanide Complexes. *Organometallics* **2006,** *25*, 3228-3237.

8. Veauthier, J. M.; Schelter, E. J.; Carlson, C. N.; Scott, B. L.; Da Re, R. E.; Thompson, J. D.; Kiplinger, J. L.; Morris, D. E.; John, K. D., Direct Comparison of the Magnetic and Electronic Properties of Samarocene and Ytterbocene Terpyridine Complexes. *Inorg. Chem.* **2008,** *47*, 5841-5849.

9. Evans, W. J.; Drummond, D. K., Reductive Coupling of Pyridazine and Benzaldehyde Azine and Reduction of Bipyridine by $(C_5Me_5)Sm(THF)_2$. *J. Am. Chem. Soc.* **1989,** *111*, 3329-3335.

10. Evans, W. J.; Davis, B. L., Chemistry of Tris(pentamethylcyclopentadienyl) f-Element Complexes, $(C_5Me_5)_3M$. *Chem. Rev.* **2002,** *102*, 2119-2136.

11. Ephritikhine, M., Recent Advances in Organoactinide Chemistry As Exemplified by Cyclopentadienyl Compounds. *Organometallics* **2013,** *32*, 2464-2488.

12. Schumann, H.; Messe-Marktscheffel, J. A.; Esser, L., Synthesis, Structure, and Reactivity of Organometallic *Chem. Rev.* **1995,** *95*, 865-986.

13. Knowles, D.; Lin, C.; Mackenzie, P.; Tsai, J.-Y.; Walters, R. W.; Beers, S.; Brown, C. S.; Yeager, W. Organic Electroluminescent Materials and Devices. US 20160240798 A1, August 18, 2016, 2016.

14. Yasukawa, T.; Kuremoto, T.; Miyamura, H.; Kobayashi, S., Asymmetric Arylation of Imines Catalyzed by Heterogeneous Chiral Rhodium Nanoparticles. *Org. Lett.* **2016,** *18*, 2716-2718.

15. Bruns, S.; Sinnwell, V.; Voss, J., Increments for ^{1}H and ^{13}C NMR Chemical Shifts in Areneboronic Acids. *Magnetic Resonance in Chemistry* **2003,** *41*, 269-272.

16. Seiple, I. B.; Su, S.; Rodriguez, R. A.; Gianatassio, R.; Fujiwara, Y.; Sobel, A. L.; Baran, P. S., Direct C-H Arylation of Electron-Deficient Heterocycles with Arylboronic Acids. *J. Am. Chem. Soc.* **2010,** *132*, 13194-13196.

17. Kalyani, D.; Dick, A. R.; Anani, W. Q.; Sanford, M. S., Scope and Selectivity in Palladium-Catalyzed Directed C–H bond Halogenation Reactions. *Tetrahedron* **2006,** *62*, 11483-11498.

18. Weiss, E., Structures of Organo Alkali Metal Complexes and Related Compounds. *Angew. Chem. Int. Ed.* **1993,** *32*, 1501-1523.

19. Ortu, F.; Liu, J.; Burton, M.; Fowler, J. M.; Formanuik, A.; Boulon, M.-E.; Chilton, N. F.; Mills, D. P., Analysis of Lanthanide-Radical Magnetic Interactions in Ce(III) 2,2'-Bipyridyl Complexes. *Inorg. Chem.* **2017,** *56*, 2496-2505.

20. Girard, P.; Namy, J. L.; Kagan, H. B., Divalent Lanthanide Derivatives in Organic Synthesis. 1. Mild Preparation of Samarium Iodide and Ytterbium Iodide and Their Use as Reducing or Coupling Agents. *J. Am. Chem. Soc.* **1980,** *102*, 2693-2698.

21. Evans, W. J.; Grate, J. W.; Choi, H. W.; Bloom, I.; Hunter, W. E.; Atwood, J. L., Solution Synthesis and Crystallographic Characterization of the Divalent Organosamarium Complexes $(C_5Me_5)_2Sm(THF)_2$ and $[(C_5Me_5)Sm(\mu\text{-}I)(THF)_2]_2$. *J. Am. Chem. Soc.* **1985,** *107*, 941-946.

22. Evans, W. J.; Grate, J. W.; Levan, K. R.; Bloom, I.; Peterson, T. T.; Doedens, R. J.; Zhang, H.; Atwood, J. L., Synthesis and X-ray Crystal Structure of Bis(pentamethylcyclopentadienyl) Lanthanide and Yttrium Halide Complexes. *Inorg. Chem.* **1986,** *25*, 3614-3619.

23. Fulmer, G. R.; Miller, A. J. M.; Sherden, N. H.; Gottlieb, H. E.; Nudelman, A.; Stoltz, B. M.; Bercaw, J. E.; Goldberg, K. I., NMR Chemical Shifts of Trace Impurities: Common Laboratory Solvents, Organics, and Gases in Deuterated Solvents Relevant to the Organometallic Chemist. *Organometallics* **2010,** *29*, 2176-2179.

24. Dolomanov, O. V.; Bourhis, L. J.; Gildea, R. J.; Howard, J. A. K.; Puschmann, H., OLEX2: A Complete Structure Solution, Refinement and Analysis Program. *J. Appl. Cryst.* **2009,** *42*, 339-341.

25. Sheldrick, G. M., SHELXT - Integrated Space-Group and Crystal-Structure Determination. *Acta Cryst.* **2015,** *A71*, 3-8.

26. Sheldrick, G. M., Crystal Structure Refinement with SHELXL. *Acta Cryst.* **2015,** *C71*, 3-8.

APPENDIX A. SYNTHESIS AND ATTEMPTED METALATION OF A TRIAMINE PINCER LIGAND

A.1 Background

Photoluminescent complexes have gained much attention for possible uses as biological imaging agents,[1] sensors,[2] phototherapy,[3] and in the solar energy conversion process.[4] In the mid-2000s, Peters reported an amido-bridged bimetallic copper system that is derived from a bis(phosphine)amide chelate ligand.[5] The ligand includes an overall anionic PNP core, ($[PNP]^-$ = bis(2-(diisobutylphosphino)phenylamide), which displays good quantum yield (ϕ > 0.65) and lifetime (τ > 10 μs). When the chelate is bound to copper, the ligand appears to create a rigid environment around the copper centers that suppresses solvent-induced exciplex formation due to sterics and limits ligand dissociation from the excited state.

It is possible to use this PNP ligand as influence for an analogous ligand system for the lanthanides. Peters' ligand features two neutral phosphine donors. This however does not match the valency needed for the lanthanides. It is necessary to change the relatively neutral and soft phosphine to a harder, anionic donor, such as a nitrogen-based base to match the harder acidic nature of the lanthanides. A core with the nitrogenous base exists in the literature, an NNN core.[6] Bimetallic lanthanide complexes can be synthesized by utilizing a bulky trianionic pincer ligand architecture based on the dimeric, luminescent copper(I) complexes developed by Peters (Figure A.1.) This ligand system features a

synthetically accessible isopropyl appendment on the outer nitrogen atoms as well as *tert*-butyl groups *para* to the central nitrogen for added steric bulk.

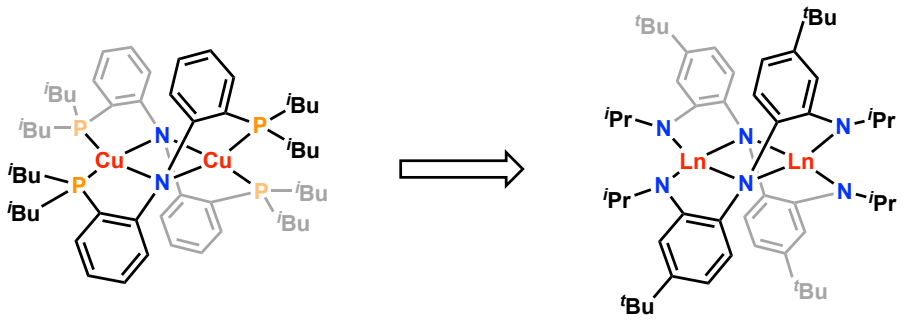

Figure A.1. Lanthanide analog of a highly luminescent bimetallic transition metal complex.

Since the lanthanides favor higher coordination numbers, the bulky pincer ligand system is expected to drive dimerization in the absence of coordinating solvents (such as tetrahydrofuran or pyridine). The trianionic ligand is redox-active and has two stable oxidized states achieved by sequential one electron oxidation (Figure A.2). Therefore, the bimetallic complex may be expected to have up to four accessible ligand-based redox states. The redox feature can allow for tuning the energies of the π or π^* orbitals via reduction or oxidation of the ligand. Therefore, these complexes can tune the metal *f*-orbital valence to the π energy of the ligand by choice of the lanthanide metal centers. With this system, MLCT, MMCT, and *f*-*d* transitions can be expected to occur.

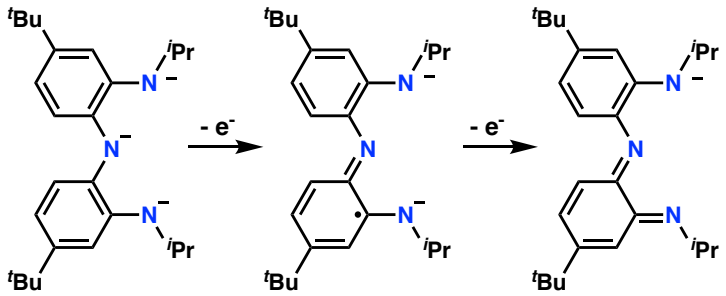

Figure A.2. Redox states of the trianionic ligand.

A.2 Results and Discussion

A.2.1 Synthesis of ^{tBu,iPr}(NNN)H$_3$

The synthesis for ligand synthesis has been previously reported.[6] However, efforts to replicate the synthesis of this ligand were problematic. The initial conversion from the diarylamine to the corresponding ortho nitration product with isoamyl nitrite yield a mixture of products. Although the desired dinitroarylamine was observed, a nitrosoamine species was observed in the FT-IR spectrum of the reaction product. Attempts to reduce the mixture of products with zinc metal and ammonium chloride led to incomplete reduction to give the triamine. Therefore, the synthesis of the ligand was redesigned to avoid these complications (Scheme A.1.). Commercially available bis(4-*tert*-butylphenyl)amine (**1**) was purified through recrystallization in methanol. The recrystallized product is protected with an acyl group (**2**) to avoid reduction at the amine.[7] Selective ortho nitration is accomplished using fuming nitric acid (**3**), then subsequent deprotection under basic conditions gives the dinitroarylamine (**4**).[7] The nitro groups are reduced with Pd/C and sodium borohydride to yield triammine, ^{tBu}(NNN)H$_5$ (**5**).[8] Reductive amination of ^{tBu}(NNN)H$_5$

using acetone and sodium cyanoborohydride yields the isopropyl-substituted pre-ligand, $^{t\text{Bu},i\text{Pr}}(\text{NNN})\text{H}_3$ (**6**).[6]

Scheme A.1. Synthesis of tridenate ligand, $^{t\text{Bu},i\text{Pr}}(\text{NNN})\text{H}_3$.

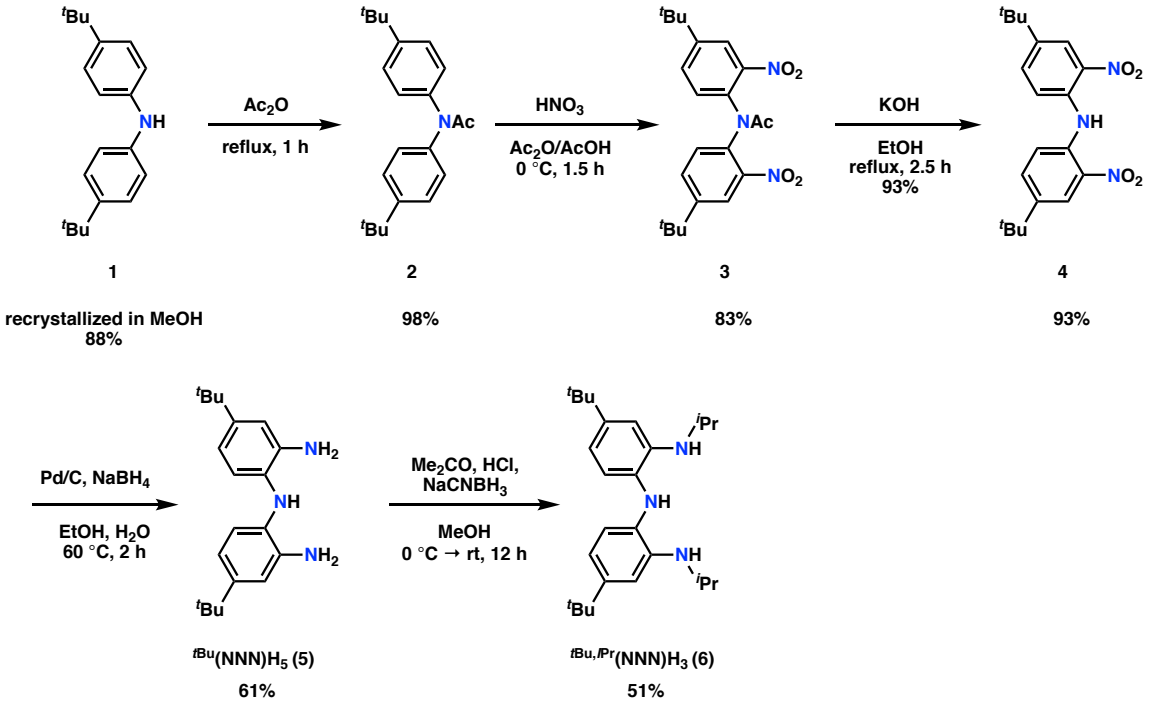

A.2.2 Metalation Studies with $^{tBu,iPr}(NNN)H_3$

Metalation of this ligand could be accomplished through many routes including protonolysis and transmetalation. Initial metalations were performed using lanthanum and yttrium. In the trivalent state, both of these metals are diamagnetic and consequently reactions involving these metals can be followed by ^{1}H NMR spectroscopy. Furthermore, yttrium features an abundant NMR-active nucleus, ^{89}Y, which would allow future further characterization. These two metals also provide an important size disparity, yttrium being on the small end of rare-

earth metals and lanthanum on the larger end, which can provide insight into the importance of metal ion size when using this ligand.

Metalation through a protonolysis route involves the use of a lanthanide starting material featuring an internal base and its reactivity with the protonated form of the ligand. A convenient and well-defined lanthanide starting material is a lanthanide trisamide. In this case, a 1:1 stoichiometric reaction between $Ln[N(TMS)_2]_3$ and $^{t\text{Bu},i\text{Pr}}(NNN)H_3$ in solvents including hexane, diethyl ether, diethyl ether/toluene, and benzene-d_6 have not been successful in metalation (Scheme A.2A). The ^{1}H NMR of these reaction products show broad resonances in both the alkyl and aromatic region indicative of the formation of oligomeric and/or polymeric species. Attempts to synthesize the tris(potassium) salt, $^{t\text{Bu},i\text{Pr}}(NNN)K_3$, have also proven unsuccessful (Scheme A.2B). Using bases such as hydride or benzyl gives incomplete deprotonation of the ligand. ^{1}H NMR of these reaction products show deprotonation of the side side-arm amines, but incomplete deprotonation of the center amine. The triamine could also be deprotonated with a stronger base such as *n*-butyllithium at low temperatures to generate the tris(lithium) salt *in situ* followed by subsequent salt metathesis with a lanthanide triiodide (Scheme A.2C). However, ^{1}H NMR indicate that formation of oligomeric species was also present, as shown by broad resonances in the spectrum, just like in the cases with the hydride and benzyl bases.

Scheme A.2. Failed metalation pathways to synthesize **6-Ln**.

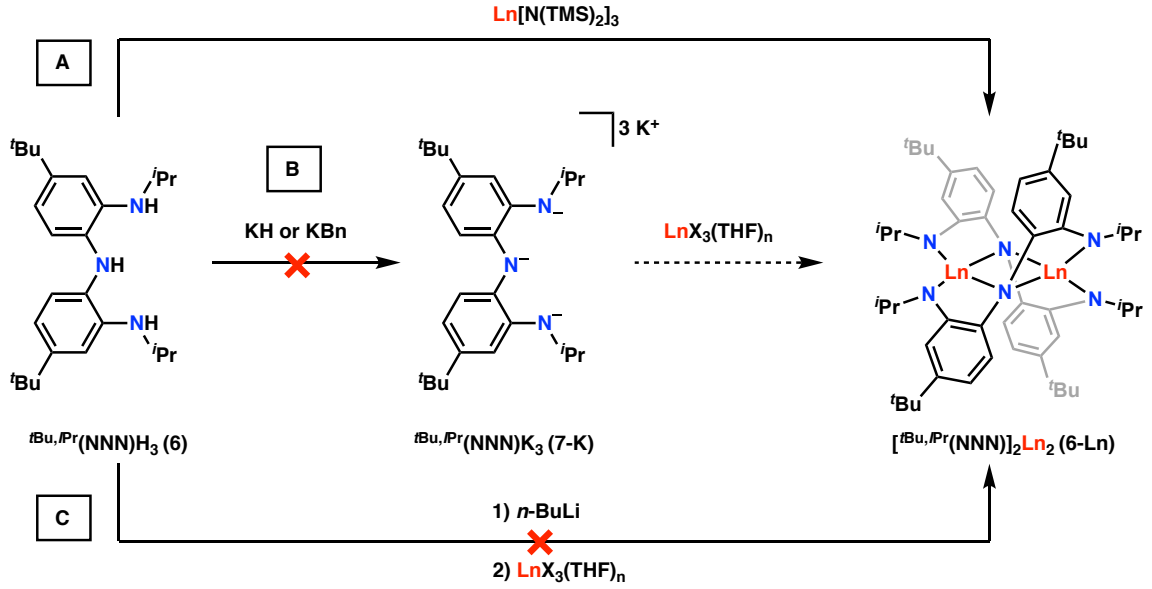

A route that holds promise for metalation includes the synthesis of the monopotassium salt, $^{t\text{Bu},i\text{Pr}}$(NNN)K (Scheme A.3). It possible to take advantage of the many redox states of the ligand to generate a stable species that can be used for metalation. Here, the full reduced form of the ligand is oxidized by electrons using the hypervalent iodide reagent, $PhI(OAc)_2$, and is simultaneously deprotonated using potassium hydride to give a monoanionic, oxidized state of the ligand.[9] Preliminary studies suggest that this route is feasible for metalation. A lanthanide triiodide can undergo salt metathesis with $^{t\text{Bu},i\text{Pr}}$(NNN)K and potentially yield a monometallic species in the presence of neutral donor ligands (e.g. pyridine) to saturate the coordination sphere. This product could then be reduced by two electrons to give the fully reduced ligand and generate the target bimetallic complex.

Scheme A.3. Pathway to synthesize **6-Ln** through monopotassium salt, **8-K**.

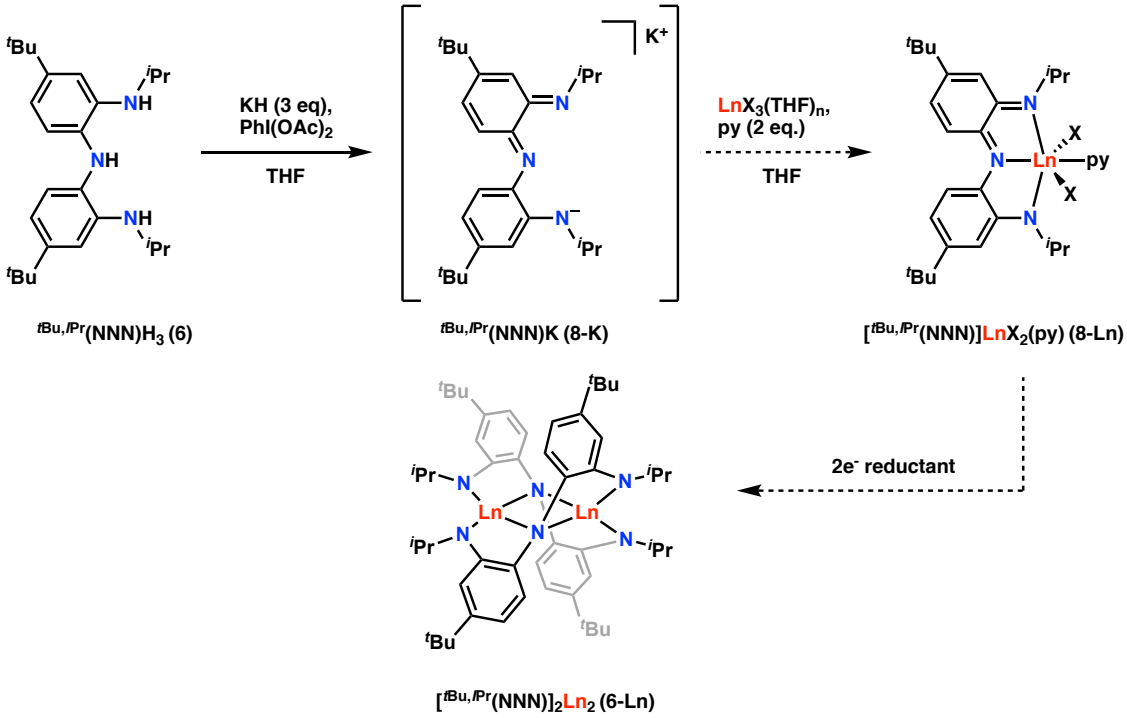

A.3 Conclusion

In summary, a new synthetic method to make a triamine, tridentate pincer ligand is reported herein. This experimental procedure generates the $^{t\text{Bu},i\text{Pr}}(\text{NNN})\text{H}_3$ ligand in five steps. Several metalation strategies including protonolysis and transmetalation have been explored but have not been fruitful. Sequential oxidation and deprotonation the fully reduced form of the ligand to yield a monoanionic salt is currently thought to be the best route to achieve a monometallic species. Two electron reduction of the monometallic complex can be completed to synthesize the bimetallic complex and be studied to investigate the photochemical and photophysical properties of bimetallic lanthanide complexes.

A.4 Experimental

A.4.1 General Considerations

Unless otherwise noted, all reagents were obtained from commercial suppliers and the syntheses and manipulations were conducted under argon with exclusion of oxygen and water using Schlenk techniques or in an inert atmosphere box (Vigor) under a dinitrogen (<0.1 ppm O_2/H_2O) atmosphere. The glovebox is equipped with two -35 °C freezers. All glassware and cannulae were stored in an oven over-night (>8 h) at a temperature of ca. 160 °C. Celite and molecular sieves were dried under vacuum at a temperature >250 °C for a minimum of 24 h. C_6D_6 was stored over 3 Å molecular sieves and then vacuum-transferred from purple sodium/benzophenone prior to use. Pentane, *n*-hexane, diethyl ether, toluene, and tetrahydrofuran were purged with UHP-grade argon (Airgas) and passed through columns containing Q-5 and molecular sieves in a solvent purification system (JC Meyer Solvent Systems). All solvents in the glovebox were stored in bottles over 3 Å molecular sieves. Acetone was dried over Drierite, then distilled and degassed. NMR spectra were obtained on a Bruker Advance III 400 MHz or Bruker Advance III HD 500 MHz spectrometer at 298 K, unless otherwise noted. ^{1}H chemical shifts are reported in δ, parts per million. ^{1}H references to the residual proton resonances of the solvent.[10] Peak position is listed, followed by peak multiplicity, integration value, and proton assignment, where applicable. Multiplicity and shape are indicated by one or more of the following abbreviations: s (singlet); d (doublet); t (triplet); q (quartet); dd (doublet of doublets); td (triplet of doublets); m (multiplet);

br (broad). Elemental analyses were determined at Robertson Microlit Laboratories (Ledgewood, NJ).

A.4.2 Synthetic Procedures

A.4.2.1 Bis(4-*tert*-butyl)phenylacetamide (**2**)

To 250 mL round-bottom flask was dissolved bis(4-*tert*-butyl)phenyl amine (6.90 g, 24.5 mmol) in acetic anhydride (50 mL) and refluxed under air for 1 h. Upon cooling, the mixture precipitated a white solid, which was washed with water and dried in vacuo to give the product as a white solid (7.78 g, 98%). ^{1}H-NMR (400 MHz, $CDCl_3$, δ): 7.36 (br, 4H, Ar-*H*), 7.19 (dt, *J* = 4.3 Hz, 2.4 Hz, 4H, Ar-*H*), 2.04 (s, 3H, C(=O)C*H*$_3$), 1.30 (s, 18H, C(C*H*$_3$)$_3$). Anal. Calcd for $C_{22}H_{29}NO$: C, 81.62 (81.69), H, 9.05 (9.04), N 4.28 (4.33). Anal. Calcd for $C_{22}H_{29}NO$: C, 81.69; H, 9.04; N, 4.33. Found: C, 81.62; H, 9.05; N 4.28.

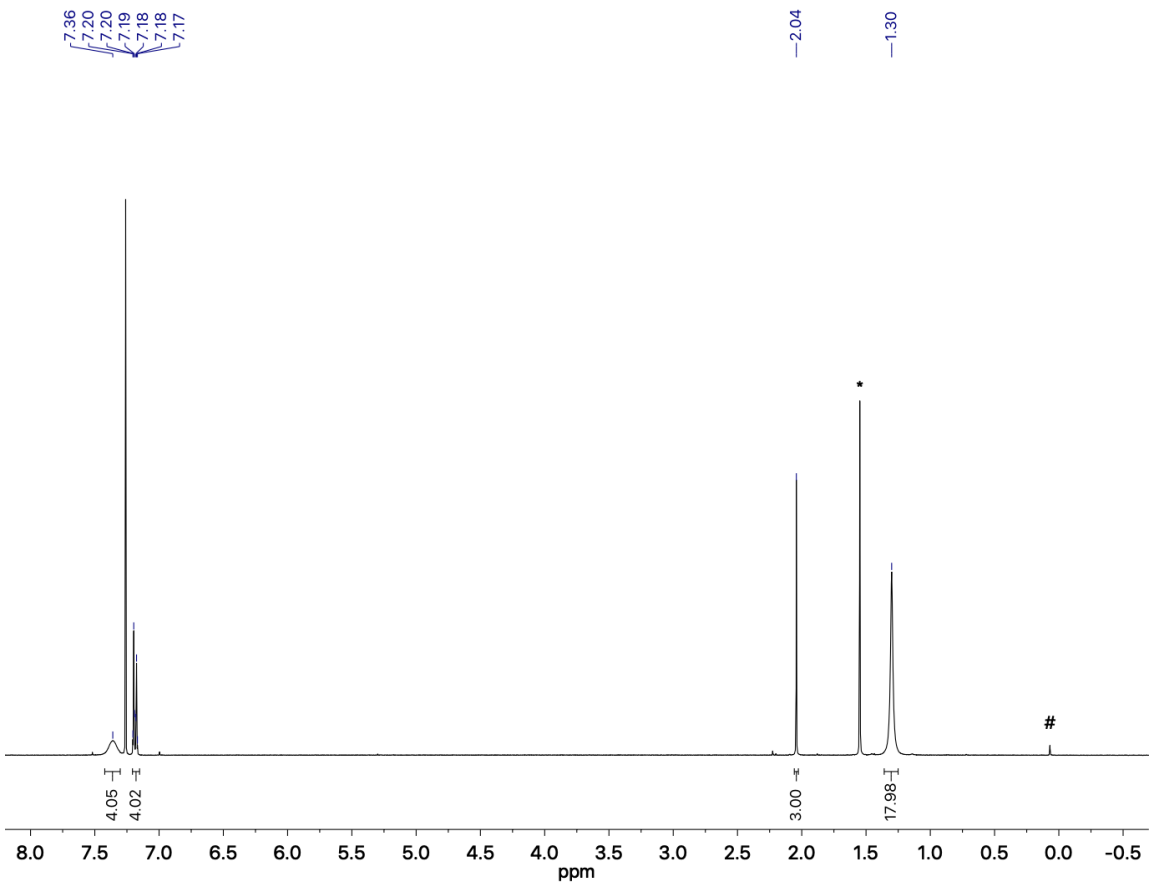

Figure A.3. ^{1}H NMR (400 MHz, $CDCl_3$) of **1**. Residual water and silicone grease are noted by * and #, respectively.

A.4.2.2 Bis(4-*tert*-butyl-2-nitrophenyl)acetamide (**3**)

To a 100 mL round-bottom flask in an ice bath was added fuming nitric acid (6.82 g, 97.4 mmol, 10.5 eq), acetic acid (16.7 mL, 292 mmol), and acetic anhydride (14.25 mL, 150 mmol). The solution was allowed to stir for 5 min before **2** (3.0 g, 9.3 mmol, 1.0 eq) was slowly added. Two extra additions of the fuming nitric acid/acetic acid/acetic anhydride solution was added 30 and 60 min, after the addition of **2**, but was prepared in a 100 mL round bottom flask and stirred for 5 min before the addition of the mixture. The light-yellow reaction solution was allowed to stir for an additional 30 min after the last addition of the acid solution.

Then, water was slowly added via squirt bottle while stirring to precipitate out a yellow solid. The solid was filtered and washed with distilled water and dried *in vacuo*. The solid recrystallized in ethanol to afford yellow crystals (3.17 g, 83%). ^{1}H-NMR (500 MHz, $CDCl_3$, δ): 8.04 (d, *J* = 1.8 Hz, 1H, Ar-*H*), 7.93 (d, *J* = 2.3 Hz, 1H, Ar-*H*), 7.70-7.69 (m, 2H, Ar-*H*), 7.53 (dd, *J* = 8.4 Hz, 2.3 Hz, 1H, Ar-*H*), 7.08 (d, *J* = 8.4 Hz, 1H, Ar-*H*), 2.00 (s, 3H, C(=O)CH_3), 1.38 (s, 9H, C(CH_3)$_3$), 1.32 (s, 9H, C(CH_3)$_3$).

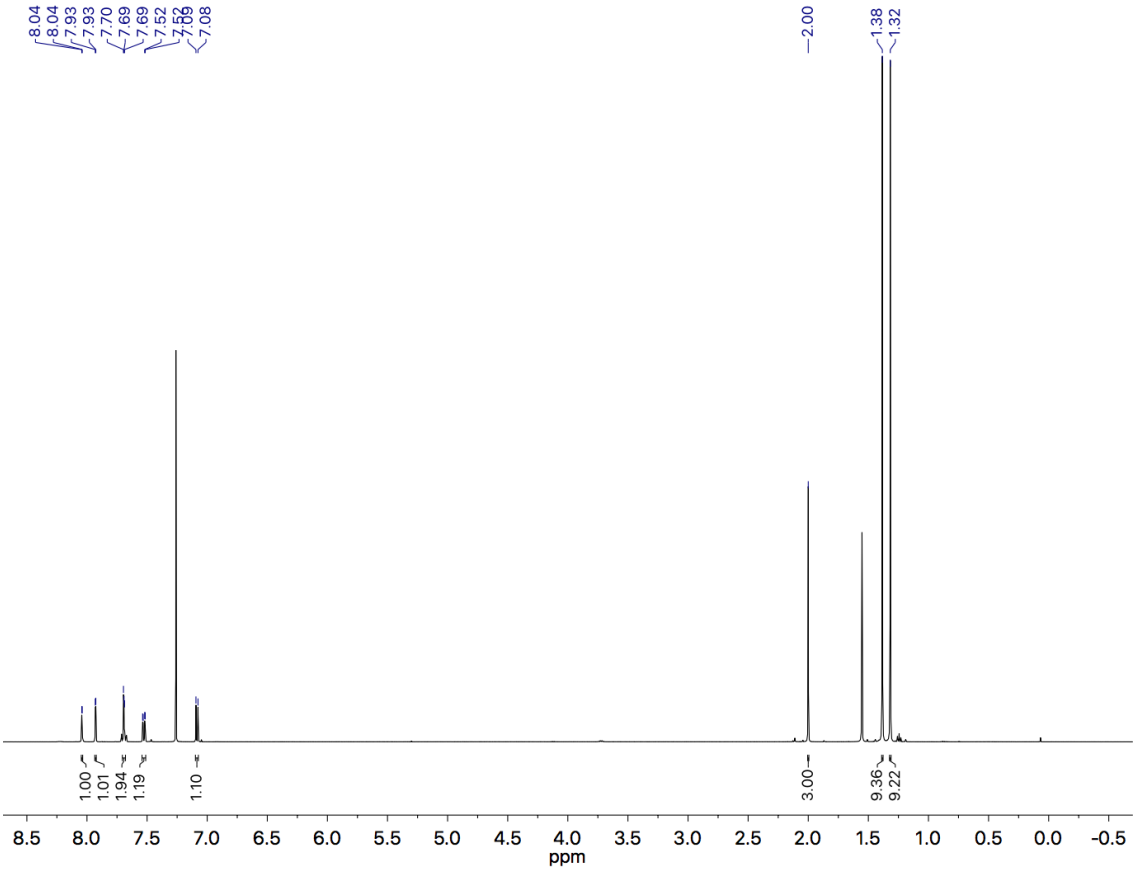

Figure A.4. ^{1}H NMR (500 MHz, $CDCl_3$) of **3**.

A.4.2.3 Bis(4-*tert*-butyl-2-nitrophenyl)amine (**4**)

To a 250 mL round-bottom flask was dissolved **3** (2.15 g, 5.20 mmol, 1.0 eq) in ethanol (100 mL) and heated to reflux under air. Then, KOH pellets (0.37 g, 6.5 mmol, 1.25 eq) was slowly added. The dark red reaction mixture was stirred at reflux for 2.5 h under air. After cooling to rt, the reaction vessel was placed in an ice bath and water was slowly added via squirt bottle while stirring to precipitate out a fine orange solid. The reaction vessel was then placed into the refrigerator for 2 h. The resulting precipitate was filtered, washed with water, and dried *in vacuo* to give the orange solid (0.65 g, 83%). *Note:* If the deprotection is not complete, the solid may be recrystallized in ethanol to give the pure product as dark red crystals. ^{1}H-NMR (500 MHz, $CDCl_3$, δ): 10.85 (s, 1H, Ar_2N-*H*), 8.18 (d, *J* = 2.1 Hz, 2H, Ar-*H*), 7.54 (dd, *J* = 8.8, 2.2 Hz, 2H, Ar-*H*), 7.50 (dd, *J* = 8.8 Hz, 2H, Ar-*H*), 1.35 (s, 18H, $C(CH_3)_3$).

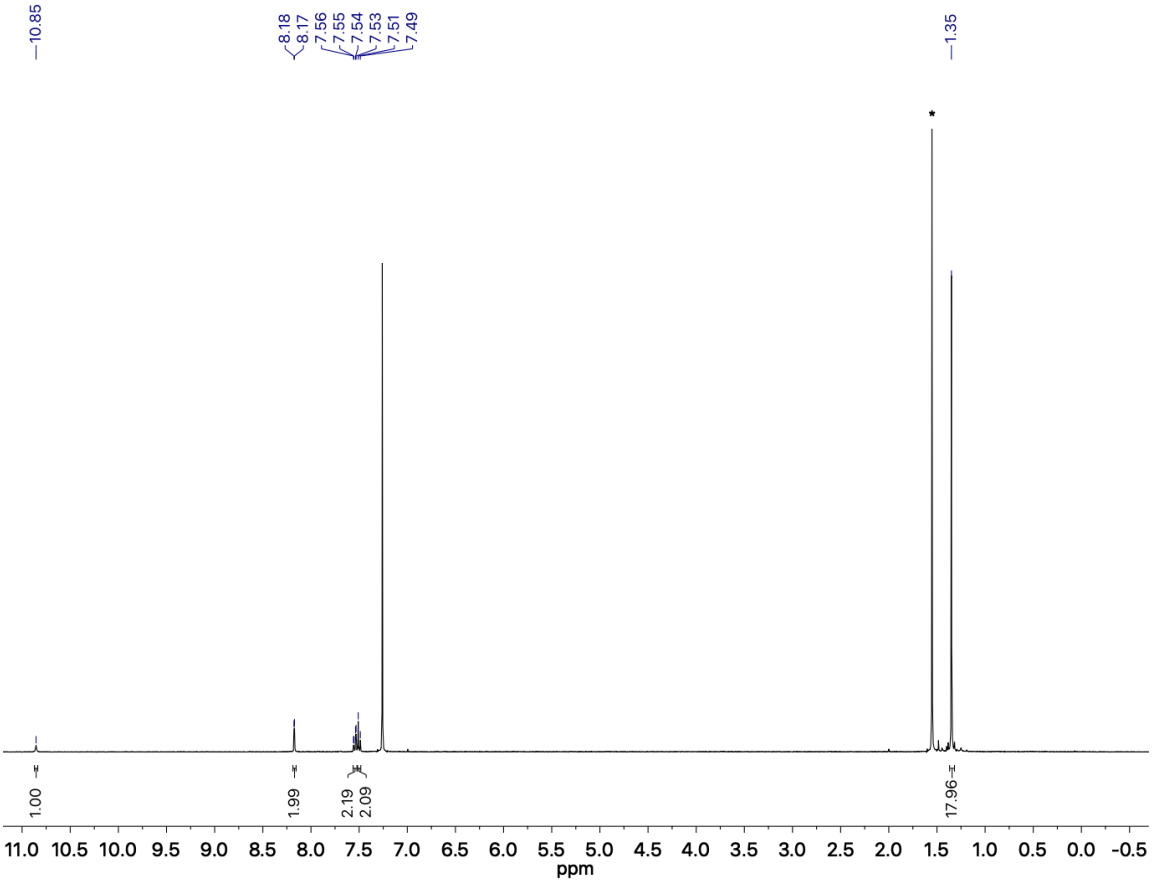

Figure A.5. ^{1}H NMR (500 MHz, $CDCl_3$) of **4**. Residual water is noted by *.

A.4.2.4 $^{t\text{Bu}}$(NNN)H_5 (**5**)

To a solution of sodium borohydride (0.204 g, 5.38 mmol, 4 eq) in H_2O (5 mL) in a 100 mL round-bottom flask was added Pd/C (0.013 g, 0.1 mol%). Then a suspension of **4** (0.500 g, 1.35 mmol, 1.0 eq) in ethanol (40 mL) was added into the reaction vessel. A reflux condenser was appended, and the mixture was heated at 60 °C for 2 h. Upon cooling to rt, the mixture was acidified to pH 3 with 1 M HCl and then basified to pH 10 with 1 M NaOH. The organic layer was extracted with diethyl ether (3 x 40 mL), washed with water (1 x 40 mL), and then with saturated sodium chloride solution (1 x 40 mL). The combined aqueous layers

were extracted once more with diethyl ether (1 x 40 mL). The organic layers were combined, dried over sodium sulfate, and the volatiles were evaporated *in vacuo*. The product was purified by column chromatography on silica gel (R_f = 0.06 in 20% EtOAc in hexanes, then 100% EtOAc) to afford the product as a dark brown solid (0.25 g, 61%). ^{1}H-NMR (500 MHz, $CDCl_3$, δ): 6.82 (d, *J* = 2.1 Hz, 2H, Ar-*H*), 6.76 (dd, *J* = 8.2, 2.2 Hz, 2H, Ar-*H*), 6.66 (d, *J* = 8.2 Hz, 2H, Ar-*H*), 4.82 (s, 1H, Ar_2N-*H*), 3.60 (s, 4H, N-H_2), 1.28 (s, 18H, $C(CH_3)_3$).

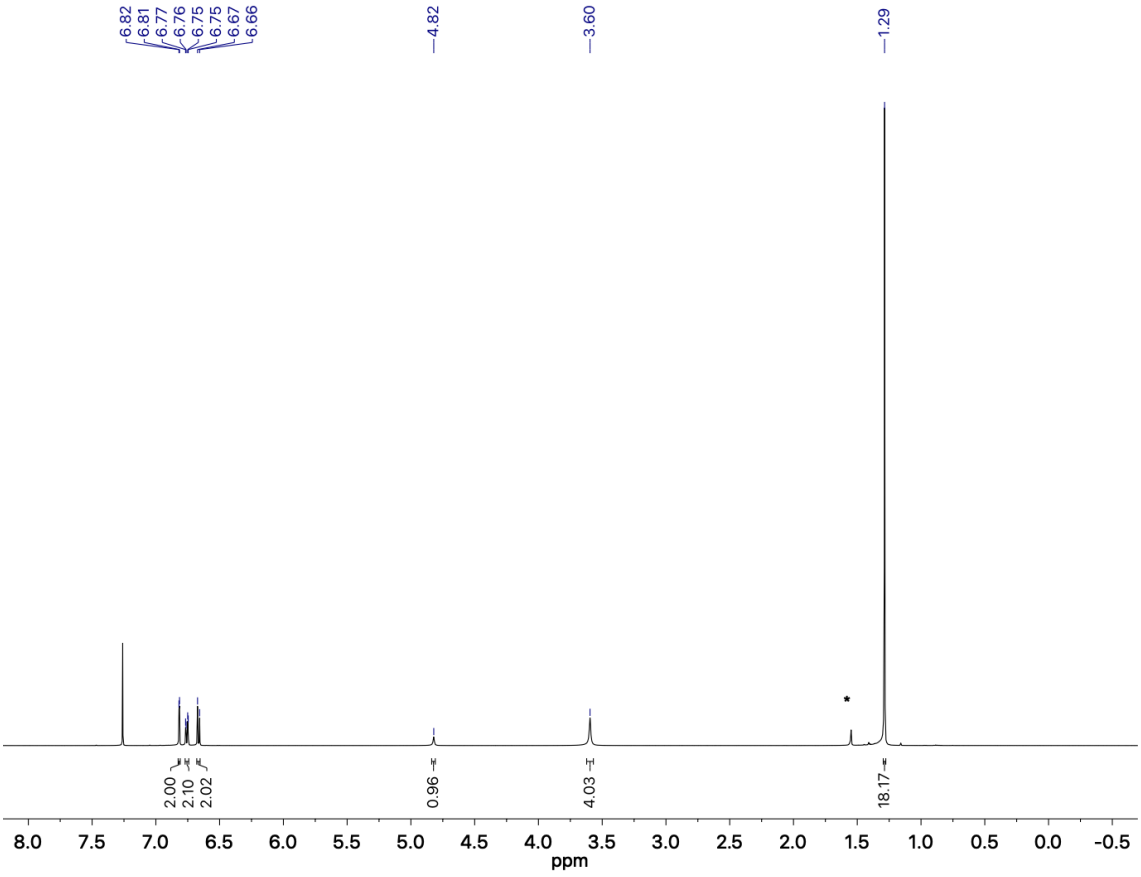

Figure A.6. ^{1}H NMR (500 MHz, $CDCl_3$) of **5**. Residual water is noted by *.

A.4.2.5 $^{t\text{Bu},i\text{Pr}}$(NNN)H_3 (**6**)

To a 500 mL Schlenk flask equipped with a stir bar was added $^{t\text{Bu}}$(NNN)H_5 (6.10 g, 19.6 mmol, 1.0 eq). Under an inert atmosphere, degassed methanol (250 mL) added via cannula into the flask. Degassed acetone (3.60 mL, 49.0 mmol, 2.5 eq) and degassed conc. HCl (1.55 mL, 49.0 mmol, 2.5 eq) were added to the flask via syringe. The dark red solution (with dark green hues, demonstrating formation of imine) was stirred in an ice/water bath for 1 h before a solid addition tube containing $NaCNBH_3$ (6.15 g, 97.9 mmol, 5.0 eq) was appended to the Schlenk flask. The solid addition tube was upended as the solution stirred. After 1 h, a white solid began to precipitate from the solution. The mixture was allowed to stir at rt for 16 h before the volatiles were evaporated *in vacuo* and the red/white residue was treated with water. The organic layer was extracted with DCM (3 x 300 mL), then dried over sodium sulfate and the volatiles were evaporated *in vacuo* and purified by column chromatography on silica gel (R_f = 0.20 in 15% EtOAc in hexanes). The red/white solid was then recrystallized in hexanes (many times) to afford a white solid (3.05 g, 39%). ^{1}H-NMR (500 MHz, $CDCl_3$, δ): 6.76 (s, 2H, Ar-*H*), 6.67 (d, *J* = 1.1 Hz, 4H, Ar-*H*), 4.76 (s, 1H, Ar_2N-*H*), 3.65 (sept, *J* = 6.2 Hz, 2H, C*H*$(CH_3)_2$), 3.51 (br, 2H, Ar(N-*H*)^{i}Pr), 1.30 (s, 9H, C(C*H*$_3)_3$), 1.19 (s, 12H, *J* = 6.2 Hz, CH(C*H*$_3)_2$). ^{1}H-NMR (500 MHz, C_6D_6, δ): 6.88 (d, *J* = 2.1 Hz, 2H, Ar-*H*), 6.80 (d, *J* = 8.1 Hz, 2H, Ar-*H*), 6.75 (dd, *J* = 8.1, 2.1 Hz, 2H, Ar-*H*), 4.78 (s, Ar_2N-*H*), 3.50 (br, 4H, Ar(N-*H*)^{i}Pr, C*H*$(CH_3)_2$), 1.34 (s, 18H, C(C*H*$_3)_3$), 0.98 (d, *J* = 6.2 Hz, 12H, CH(C*H*$_3)_2$).

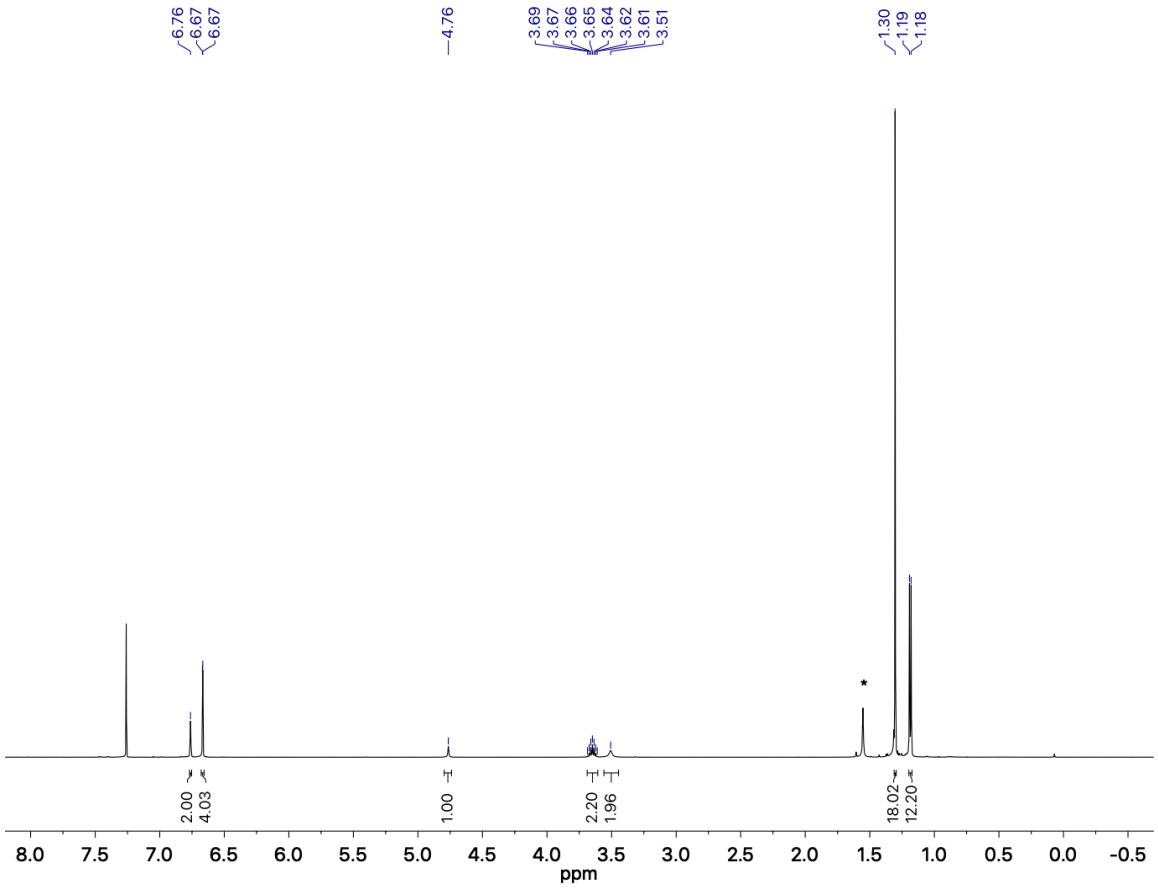

Figure A.7. ^{1}H NMR (500 MHz, $CDCl_3$) of **6**. Residual water is noted by *.

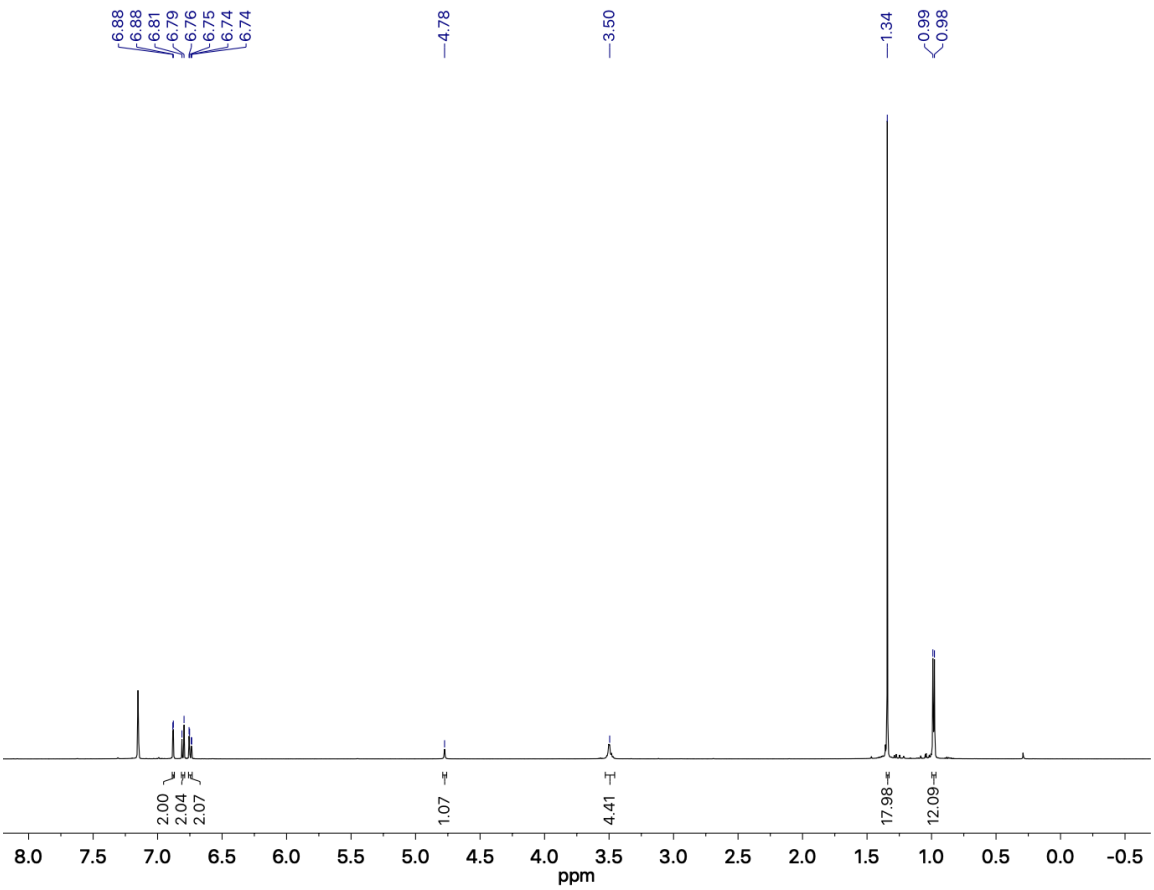

Figure A.8. ^{1}H NMR (500 MHz, C_6D_6) of **6**.

A.5 References

1. Lo, K. K.-W., Luminescent Rhenium(I) and Iridium(III) Polypyridine Complexes as Biological Probes, Imaging Reagents, and Photocytotoxic Agents. *Acc. Chem. Res.* **2015,** *48*, 2985-2995.

2. Keefe, M. H.; Benkstein, K. D.; Hupp, J. T., Luminescent Sensor Molecuels Based on Coordinated Metals: A Review of Recent Developments. *Coord. Chem. Rev.* **2000,** *205*, 201-228.

3. Zamora, A.; Vigueras, G.; Rodríguez, V.; Santana, M. D.; Ruiz, J., Cyclometalated Iridium(III) Luminescent Complexes in Therapy and Phototherapy. *Coord. Chem. Rev.* **2018,** *360*, 34-76.

4. Buldt, L. A.; Wenger, O. S., Chromium Complexes for Luminescence, Solar Cells, Photoredox Catalysis, Upconversion, and Phototriggered NO Release. *Chem. Sci.* **2017,** *8*, 7359-7367.

5. Harkins, S. B.; Peters, J. C., A Highly Emissive Cu_2N_2 Diamond Core Complex Supported by a $[PNP]^-$ Ligand. *J. Am. Chem. Soc.* **2005,** *127*, 2030-2031.

6. Munhá, R. F.; Zarkesh, R. A.; Heyduk, A. F., Tuning the Electronic and Steric Parameters of a Redox-Active Tris(amido) Ligand. *Inorg. Chem.* **2013,** *52*, 11244-11255.

7. Frantz, D. K.; Linden, A.; Baldridge, K. K.; Siegel, J. S., Molecular Spur Gears Comprising Triptycene Rotators and Bibenzimidazole-Based Stators. *J. Am. Chem. Soc.* **2012,** *134*, 1528-1535.

8. McNab, H.; Smith, G. S., The Thermolysis of Polyazapentadienes. Part 5. Degenerate Rearrangement of Aryliminoiminyl Radicals: A ^{15}N-Labelling Study. *J. Chem. Soc. Perkin Trans. 1* **1984**, 381-384.

9. Szigethy, G.; Shaffer, D. W.; Heyduk, A. F., Coordination Effects on Electron Distributions for Rhodium Complexes of the Redox-Active Bis(3,5-di-*tert*-butyl-2-phenolate)amide Ligand. *Inorg. Chem.* **2012,** *51*, 12606-12618.

10. Fulmer, G. R.; Miller, A. J. M.; Sherden, N. H.; Gottlieb, H. E.; Nudelman, A.; Stoltz, B. M.; Bercaw, J. E.; Goldberg, K. I., NMR Chemical Shifts of Trace Impurities: Common Laboratory Solvents, Organics, and Gases in Deuterated Solvents Relevant to the Organometallic Chemist. *Organometallics* **2010,** *29*, 2176-2179.

APPENDIX B. SYNTHESIS AND METALATION OF AN IMIDOPHOSPHORANE LIGAND

B.1 Note on Collaboration

This chapter contains X-ray crystals structures that were solved by Dr. John Bacsa. The work completed here is collaborative with ligand synthesis completed by Ms. Natalie Rice.

B.2 Background

It is well-known that samarium diiodide has capabilities to reduce organic bromides and iodides, the reduction of organic chlorides is difficult. In a report from Inanaga in the 1980s, samarium diiodide solutions in THF were shown to reduce alkyl and aryl halides with the addition of hexamethylphosphoramide (HMPA).[1] Later studies by McDonald show that tripyrrolidinophosphoric acid triamide (TPPA) (Figure B.1) can also be used to enhance the reactivity of samarium diiodide.[2]

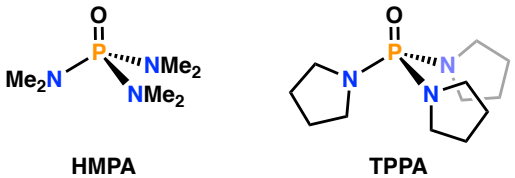

Figure B.1. Structures of HMPA and TPPA.

TPPA has a slight advantage over HMPA due to its greater Lewis basicity. The versatility of this reagent in organic synthesis is further enhanced by its ability

to promote both one- and two-electron reduction processes. HMPA additives have been shown to increase the reducing ability of samarium diiodide in part by dissociating samarium diiodide aggregates in solution, allowing for extra equivalents of amide additive to perturb the electron-donating orbital of the metal, raising its energy and thus making the Sm(2+)/Sm(3+) reduction potential more negative.[3] Cossy and Portella have also shown that HMPA, under UV irradiation, is an efficient electron donor in the case of cyclizing δ,ϵ-unsaturated ketones.[4] Ogawa reports that visible light increases the reduction potential of samarium diiodide enough to reduce organic chlorides.[5] The UV-vis spectrum in THF shows absorbances at 565 and 617 nm which is identified as a $4f^6 \rightarrow 4f^5 5d^1$ transition and the reduction process is thought to involve a single-electron transfer from the photoexcited SmI_2 species to the organic chloride.[6] Coupling these systems together, it may be expected that HMPA analogs can be photochemically activated if used as a ligand in samarium systems (Figure B.2).

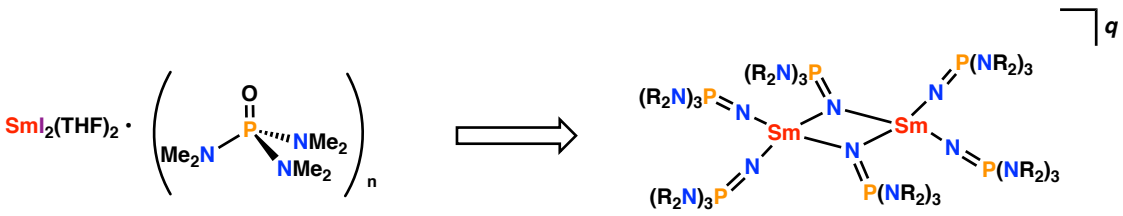

Figure B.2. Lanthanide bimetallic bearing an HMPA-like ligand.

A bimetallic complex with an anionic analog of HMPA can be envisioned. Imidophosphoranes, $[(R_2N)_3P{=}N]^-$, are 1σ and 2π donors and bind to metals with

a strong nitrogen donor atom but also provides steric control of the substituents at the phosphorus atom. This weak field ligand will allow for changing the relative energies of the 4f orbitals into the 5d orbital manifold, which will change the excitation energy needed for an electronic transition and make excitations more accessible.

B.3 Results and Discussion

B.3.1 Synthesis of $K_4[(pip)_3PN]_4$

The tris(piperidinyl)imidophosphorane ligand, $[NP(pip)_3]^-$, is prepared as the potassium salt, $K[NP(pip)_3]$ (**1-K**) by literature procedures.[7] Tris(piperdinyl)phopsphine is first oxidized with trimethylsilyl azide and then desilylated using methanol. The resulting imine is deprotonated with potassium benzyl to yield the potassium salt, **1-K**, which forms a tetrameric cluster. After evaporating the reaction volatiles *in vacuo*, the residue is taken up in THF, filtered through a fine-porosity sintered glass frit packed with Celite, and is precipitated from solution at -35 °C. After decantation, **1-K** is obtained as a white solid.

Scheme B.1. Synthesis of **1-K**.

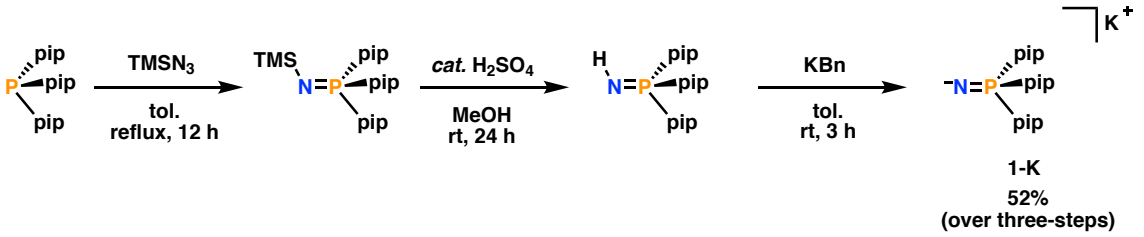

B.3.2 Synthesis and Characterization of Samarium Complexes

Initially, **1-K** is reacted with $SmI_3(THF)_{3.5}$ in a three to one ratio respectively, agitated manually periodically for four hours, then let to react at room temperature for a total of 16 h. The product is extracted in *n*-pentane, precipitated from solution at -35 °C, and XRD quality crystals are grown via hexane evaporation. Previously results in the group for analogous reactions yielded the formation of lanthanide dimers, for which there are two bridging and two terminal ligands, $[Ln_2\{(pip)_3PN\}_6]$. However, this reaction resulted in incomplete salt metathesis, giving the samarium monoiodide dimer, $[Sm_2\{(pip)_3PN\}_5I]$, **2-Sm**, Figure B.3.

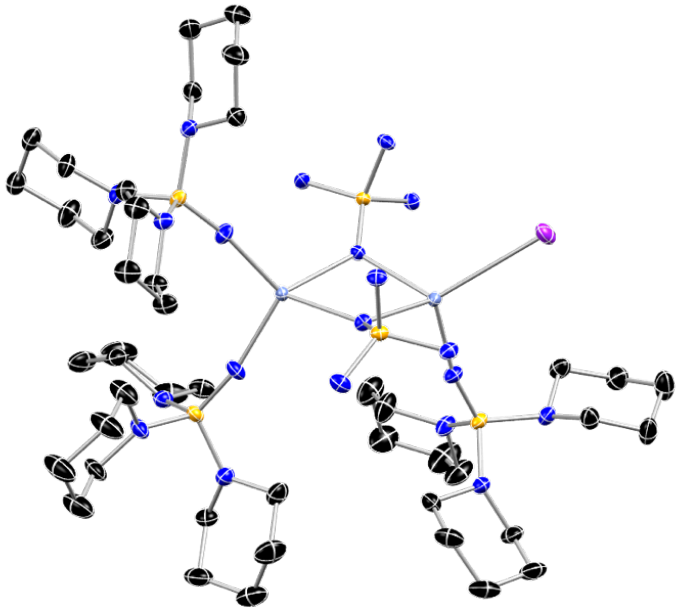

Figure B.3. Molecular structure of **2-Sm** with thermal ellipsoids shown at 50% probability. H atoms and bridging piperidine carbons have been omitted for clarity.

Attempts to replicate the synthesis of the samarium monoiodide dimer were completed by the reaction of one equivalent of $SmI_3(THF)_{3.5}$ with 2.5 equivalents of the ligand salt using the same workup procedure and crystallization conditions

as previously described. This reaction gave a neutral tetrahomoleptic samarium monometallic complex, **3-Sm**, Figure B.4. This complex crystallizes with two distinct geometries in the asymmetric unit cell. The potassium atom on the one of the geometries is supported by a capping THF molecule and three of the imido nitrogens. The other is not capped by THF and is only supported by two imido nitrogens.

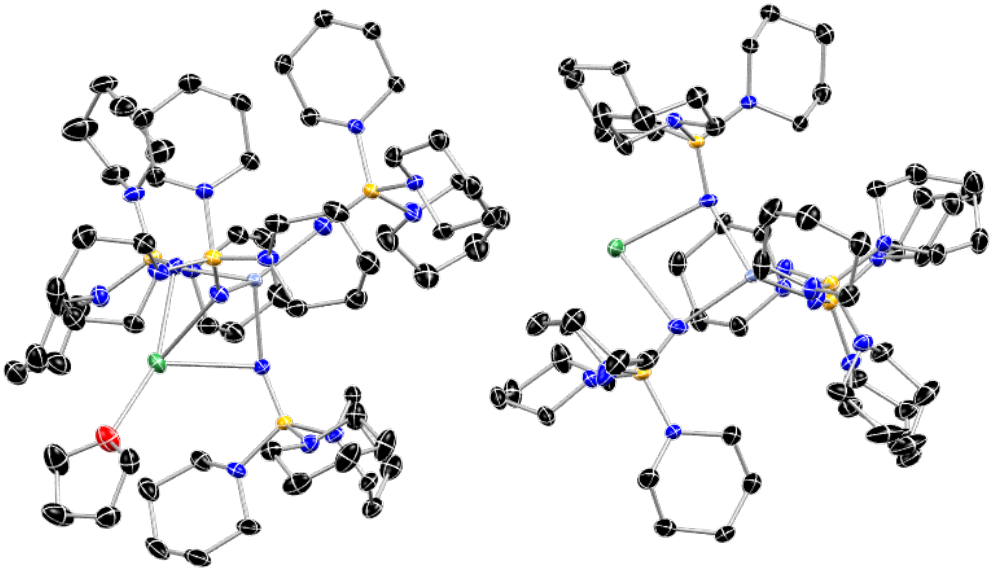

Figure B.4. Molecular structure of **3-Sm** with thermal ellipsoids shown at 50% probability. H atoms and bridging piperidine carbons have been omitted for clarity.

Following further purification of the ligand salt, the salt metathesis of $SmI_3(THF)_{3.5}$ with three equivalents of ligand, stirring at room temperature for 24 h in addition to the manual agitation method previously described for 16 h resulted in the sole isolation of the *hexakis* samarium dimer, $[Sm_2\{(pip)_3PN\}_6]$, **4-Sm**, Figure B.5.

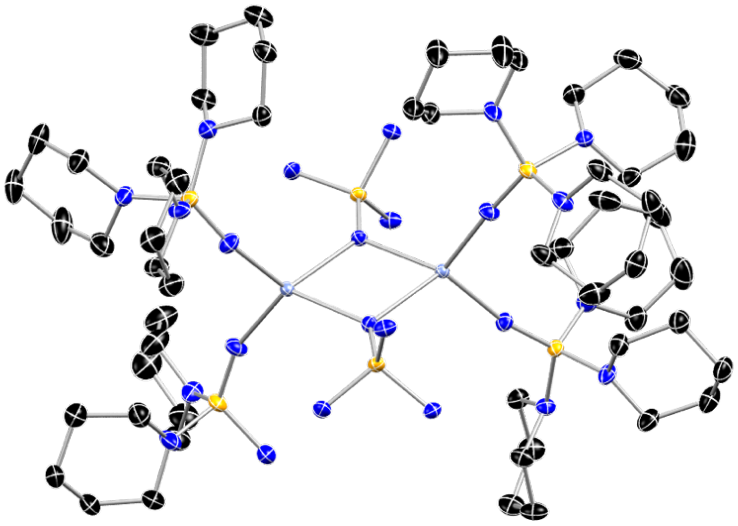

Figure B.5. Molecular structure of **4-Sm** with thermal ellipsoids shown at 50% probability. H atoms and bridging piperidine carbons have been omitted for clarity.

B.3.3 Synthesis and X-ray Crystal Structure of [Yb_2{$(pip)_3PN$}$_5$]

The short atomic distances between the lanthanide metal centers is encouraging for the study of lanthanide photochemistry, as *f-d* transitions may be present in lanthanides with low-lying excited states, such as samarium, europium, ytterbium, and other multinuclear lanthanide complexes. Due to the low redox couple in samarium, europium, and ytterbium, these lanthanides have accessible divalent states. The lanthanide diiodide THF adducts, $LnI_2(THF)_2$ (Ln = Sm, Eu, Yb), may also be used. The divalent lanthanides can be used to explore lower energy *f-d* transitions. Due to the very negative redox couple of Sm(2+/3+), a less reducing lanthanide, ytterbium, was initially explored to prevent the formation of by-products from spontaneous redox events.

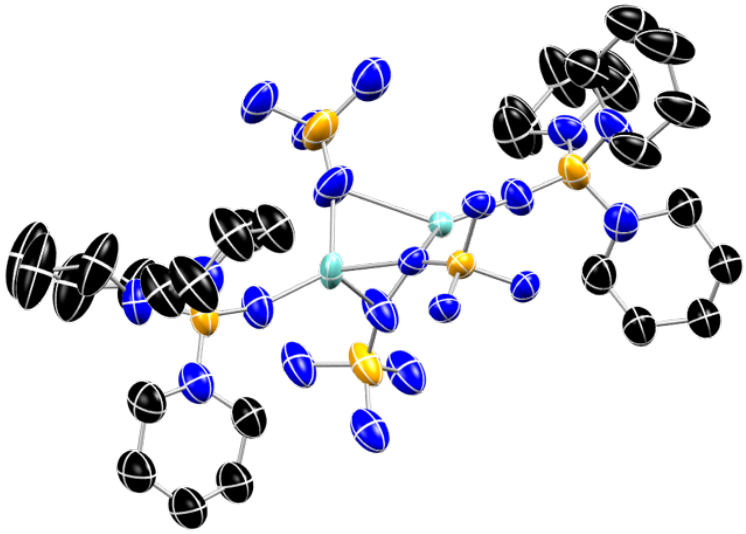

Figure B.6. Molecular structure of **5-Yb** with thermal ellipsoids shown at 50% probability. H atoms and bridging piperidine carbons have been omitted for clarity.

The reaction of $YbI_2(THF)_2$ with **1-K** resulted in a unique bimetallic compound in which the metals are bridged by three ligands and has two terminal ligands, **5-Yb**, Figure B.6. Conceivably, the three bridging ligands bring the two metal ions strikingly close together exhibiting an interatomic distance of 3.008 Å. Considering valence electron count, this bimetallic is a mixed valent Yb(2+)/Yb(3+) species, suggesting that an auto-redox event occurred during the reaction. This mixed valent complex is potentially interesting for MMCT investigations. Comparing the Yb-N distances, one Yb-N set has an average distance of 2.493(9) Å and the other with an average Yb-N distance of 2.200(8) Å. Since divalent ytterbium has a larger ionic radius than trivalent ytterbium, the crystal structure suggests that the electron is localized yielding two discrete valence states. This complex might allow for the study of how the metal the interaction and overlap of valence orbitals affects bonding, thermodynamics, and reactivity.

B.4 Conclusion

A novel anionic imidophosphorane ligand was used to synthesize systems to explore the photochemistry of bimetallic lanthanide systems. A variety of monometallic and homobimetallic samarium systems were synthesized in addition to an interesting homobimetallic ytterbium complex. This complex presents a unique opportunity to study the photochemistry of bimetallic lanthanide systems in addition to problems in bonding in the lanthanides.

B.5 Experimental

B.5.1 General Considerations

Unless otherwise noted, all reagents were obtained from commercial suppliers and the syntheses and manipulations were conducted under argon with exclusion of oxygen and water using Schlenk techniques or in an inert atmosphere box (Vigor) under a dinitrogen (< 0.1 ppm O_2/H_2O) atmosphere. The glovebox is equipped with two -35 °C freezers. All glassware and cannulae were stored in an oven over-night (> 8 h) at a temperature of ca. 160 °C. Celite and molecular sieves were dried under vacuum at a temperature >250 °C for a minimum of 24 h. C_6D_6 was stored over 3 Å molecular sieves and then vacuum-transferred from purple sodium/benzophenone prior to use. Pentane, *n*-hexane, diethyl ether, toluene, and tetrahydrofuran were purged with UHP-grade argon (Airgas) and passed through columns containing Q-5 and molecular sieves in a solvent purification system (JC Meyer Solvent Systems). All solvents in the glovebox were stored in bottles over 3 Å molecular sieves. Methanol was dried by refluxing magnesium turnings

activated with iodine for 12 h, then distilled and stored over 3 Å molecular sieves. THF adducts of lanthanide triiodide starting materials were prepared according to literature procedures.[8] Potassium *tert*-butoxide was sublimed prior to use. Potassium benzyl was prepared according to a published procedure.[9] Tris(piperidinyl)phosphine was prepared to a published procedure.[10] Potassium tris(piperidinyl)imidophosphorane was synthesized according to a reported procedure.[7] UV-vis-NIR spectra were obtained on a Schimadzu UV-3101PC. X-ray structural determinations were performed at the Georgia Institute of Technology on a Bruker D8 Venture diffractometer.

B.5.2 Synthetic Procedures

B.5.2.1 $[Sm_2\{(pip)_3PN\}_5I]$ (**2-Sm**)

In a 20 mL scintillation vial charged with $SmI_3(THF)_{3.5}$ (0.230 g, 0.294 mmol, 1.0 eq), $K[(pip)_3PN]$ (0.304 g, 0.881 mmol, 3.0 eq) was added as a solution in THF (8 mL). A white precipitate formed immediately with a concomitant color change from yellow to colorless. The reaction mixture was stirred with a glass stir bar for 24 h. The mixture was filtered through a fine porosity, sintered glass frit, the filtrate was reduced to a residue *in vacuo* and was then triturated three times with *n*-pentane (3 x 2 mL). The resulting solid was taken up in *n*-pentane and filtered through a pipette filter with Celite, the solution as concentrated to less than 1 mL and XRD quality crystals were grown at room temperature via the slow evaporation of hexanes from a solution of product in a 4 mL vial inside a 20 mL vial with paratone oil in the outer vial.

B.5.2.2 K[Sm{$(pip)_3PN$}$_4$](THF)K[Sm{$(pip)_3PN$}$_4$] (**3-Sm**)

In a 20 mL scintillation vial charged with $SmI_3(THF)_{3.5}$ (0.170 g, 0.310 mmol, 1.0 eq), K[$(pip)_3PN$] (0.313 g, 0.930 mmol, 3.0 eq) was added as a solution in THF (8 mL). A white precipitate formed immediately with a concomitant color change from yellow to colorless. The reaction mixture was stirred with a glass stir bar for 24 h. The mixture was filtered through a fine porosity, sintered glass frit, the filtrate was reduced to a residue *in vacuo* and was then triturated three times with *n*-pentane (3 x 2 mL). The resulting solid was taken up in *n*-pentane and filtered through a pipette filter with Celite, the solution as concentrated to less than 1 mL and XRD quality crystals were grown at room temperature via the slow evaporation of hexanes from a solution of product in a 4 mL vial inside a 20 mL vial with paratone oil in the outer vial.

B.5.2.3 [Sm_2{$(pip)_3PN$}$_6$] (**4-Sm**)

In a 20 mL scintillation vial charged with $SmI_3(THF)_{3.5}$ (0.230 g, 0.294 mmol, 1.0 eq), K[$(pip)_3PN$] (0.304 g, 0.881 mmol, 3.0 eq) was added as a solution in THF (8 mL). A white precipitate formed immediately with a concomitant color change from yellow to colorless. The reaction mixture was stirred with a glass stir bar for 24 h. The mixture was filtered through a fine porosity, sintered glass frit, the filtrate was reduced to a residue *in vacuo* and was then triturated three times with *n*-pentane (3 x 2 mL). The resulting solid was taken up in *n*-pentane and filtered through a pipette filter with Celite, the solution as concentrated to less than 1 mL and XRD quality crystals were grown at room temperature via the slow evaporation

of hexanes from a solution of product in a 4 mL vial inside a 20 mL vial with paratone oil in the outer vial.

B.5.2.4 $[Yb_2\{(pip)_3P\}_5]$ (**4-Yb**)

In a 20 mL scintillation vial charged with $YbI_2(THF)_2$ (0.255 g, 0.447 mmol, 1.0 eq), K[(pip)$_3$PN] (0.309 g, 0.893 mmol, 2.0 eq) was added as a solution in THF (8 mL). A white precipitate formed immediately. The reaction mixture was stirred with a glass stir bar for 24 h. The mixture was filtered through a fine porosity, sintered glass frit, the filtrate was reduced to a residue *in vacuo* and was then triturated three times with *n*-pentane (3 x 2 mL). The resulting residue was taken up in *n*-pentane and filtered through a pipette filter with Celite, the solution as concentrated to less than 1 mL, and XRD quality crystals were grown at room temperature via the slow evaporation of hexanes from a solution of product in a 4 mL vial inside a 20 mL vial with paratone oil in the outer vial.

B.5.3 X-ray Diffraction Data

B.5.3.1 $[Sm_2\{(pip)_3PN\}_5I]$ (**2-Sm**)

Experimental. Single colorless, prism-shaped crystals of **2-Sm** were crystallized from a concentrated solution in pentane at -35 °C. A suitable crystal 0.130×0.327×0.291 mm^2 was selected and mounted on a loop with paratone oil on a Bruker D8 Venture diffractometer with MO Kα radiation and PHOTON II detector. The crystal was kept at 100(2) K during data collection. Using Olex2,[11] the structure was solved with ShelXT[12] structure solution program using Intrinsic

Phasing and refined with ShelXL[13] refinement package using Least Squares Minimization.

Crystal Data. $C_{81}H_{163}IN_{20}P_5Sm_2$ (M = 2000.76 g/mol): triclinic, space group P-1 (no. 2), a = 14.8950(8) Å, b = 14.8860(8) Å, c = 25.6496(13) Å, α = 100.405(2)°, β = 90.628(2)°, γ = 117.106(2)°, V = 4951.0(5) Å^3, Z = 2, T = 100(2) K, μ(Mo Kα) = 1.616 mm^{-1}, *Dcalc* = 1.342 g/cm^3, 125386 reflections measured (4.338° ≤ 2θ ≤ 72.648°), 47602 unique (R_{int} = 0.0353, R_{sigma} = 0.0475) which were used in all calculations. The final R_1 was 0.0377 (I > 2σ(I)) and wR_2 was 0.0951 (all data).

B.4.3.2 K[Sm{(pip)$_3$PN}$_4$](THF)K[Sm{(pip)$_3$PN}$_4$] (**3-Sm**)

Experimental. Single colorless, prism-shaped crystals of **3-Sm** were crystallized from a concentrated solution in pentane at -35 °C. A suitable crystal 0.575×0.364×223 mm^2 was selected and mounted on a loop with paratone oil on a Bruker D8 Venture diffractometer with MO Kα radiation and PHOTON II detector. The crystal was kept at 100(2) K during data collection. Using Olex2,[11] the structure was solved with ShelXT[12] structure solution program using Intrinsic Phasing and refined with ShelXL[13] refinement package using Least Squares Minimization.

Crystal Data. $C_{124}H_{248}K_2N_{32}OP_8Sm_2$ (M = 2830.19 g/mol): triclinic, space group P-1 (no. 2), a = 13.3158(8) Å, b = 20.797(14) Å, c = 26.3842(17) Å, α = 90.315(3)°, β = 94.147(2)°, γ = 93.069(3)°, V = 7277.6(8) Å^3, Z = 2, T = 100(2) K, μ(Mo Kα) = 1.001 mm^{-1}, *Dcalc* = 1.292 g/cm^3, 229680 reflections measured (5.112° ≤ 2θ ≤ 61.994°), 46373 unique (R_{int} = 0.0638, R_{sigma} = 0.0548) which were

used in all calculations. The final R_1 was 0.0414 (I > 2σ(I)) and wR_2 was 0.1031 (all data).

B.5.3.3 $[Sm_2\{(pip)_3PN\}_6]$ (**4-Sm**)

Experimental. Single colorless, prism-shaped crystals of **4-Sm** were crystallized from a concentrated solution in pentane at -35 °C. A suitable crystal 0.326×0.321×0.272 mm^2 was selected and mounted on a loop with paratone oil on a Bruker D8 Venture diffractometer with MO Kα radiation and PHOTON II detector. The crystal was kept at 100(2) K during data collection. Using Olex2,[11] the structure was solved with ShelXT[12] structure solution program using Intrinsic Phasing and refined with ShelXL[13] refinement package using Least Squares Minimization.

Crystal Data. $C_{90}H_{180}N_{24}P_6Sm_2$ (M = 2085.09 g/mol): monoclinic, space group $P2_1/c$ (no. 14), a = 15.4034(6) Å, b = 24.8126(11) Å, c = 29.2672(12) Å, β = 99.8760(15)°, V = 11020.1(8) $Å^3$, Z = 4, T = 100(2) K, μ(Mo Kα) = 1.193 mm^{-1}, *Dcalc* = 1.257 g/cm^3, 285162 reflections measured (4.322° ≤ 2θ ≤ 62.044°), 35126 unique (R_{int} = 0.0471, R_{sigma} = 0.0276) which were used in all calculations. The final R_1 was 0.0304 (I > 2σ(I)) and wR_2 was 0.0782 (all data).

B.5.3.4 $[Yb_2\{(pip)_3PN\}_5]$ (**5-Yb**)

Experimental. Single green, prism-shaped crystals of **5-Yb** were crystallized from a concentrated solution in pentane at -35 °C. A suitable crystal 0.429×0.214×0.177 mm^2 was selected and mounted on a loop with paratone oil on a Bruker D8 Venture diffractometer with MO Kα radiation and PHOTON II detector. The crystal was kept at 100(2) K during data collection. Using Olex2,[11]

the structure was solved with ShelXT[12] structure solution program using Intrinsic Phasing and refined with ShelXL[13] refinement package using Least Squares Minimization.

Crystal Data. $C_{75}H_{150}IN_{20}P_5Yb_2$ (M = 1833.07 g/mol): orthorhombic, space group $Pna2_1$ (no. 33), a = 25.5413(16) Å, b = 24.1508(14) Å, c = 14.0691 Å, V = 8678.4(9) Å^3, Z = 4, T = 100(2) K, μ(Mo Kα) = 2.286 mm^{-1}, *Dcalc* = 1.403 g/cm^3, 224846 reflections measured (4.626° ≤ 2θ ≤ 60.148°), 25420 unique (R_{int} = 0.0825, R_{sigma} = 0.0507) which were used in all calculations. The final R_1 was 0.0921 (I > 2σ(I)) and wR_2 was 0.2800 (all data).

3.6 References

1. Inanaga, J.; Ishikawa, M.; Yamaguchi, M., A Mild and Convenient Method for the Reduction of Organic Halides by Using a SmI_2-THF Solution in the Presence of Hexamethylphosphoric Triamide (HMPA). *Chem. Lett.* **1987,** *16*, 1485-1486.

2. McDonald, C. E.; Ramsey, J. D.; Sampsell, D. G.; Butler, J. A.; Cecchini, M. R., Tripyrrolidinophosphoric Acid Triamide as an Activator in Samarium Diiodide Reductions. *Org. Lett.* **2010,** *12*, 5178-5181.

3. Molander, G. A.; McKie, J. A., Samarium(II) Iodide-Induced Reductive Cyclization of Unactivated Olefinic Ketones. Sequential Radical Cyclizations/Intermolecular Nucleophilic Addition and Substitution Reactions. *J. Org. Chem.* **1992,** *57*, 3132-3139.

4. Belotti, D.; Cossy, J.; Pete, J. P.; Portella, C., Synthesis of Bicyclic Cyclopentanols by Photoreductive Cyclization of *J. Org. Chem.* **1986,** *51*, 4196-4200.

5. Ogawa, A.; Sumino, Y.; Nanke, T.; Ohya, S.; Sonoda, N.; Hirao, T., Photoinduced Reduction and Carbonylation of Organic Chlorides with Samarium Diiodide. *J. Am. Chem. Soc.* **1997,** *119*, 2745-2746.

6. Okaue, Y.; Isobe, T., Characterizations of Divalent Lanthanoid Iodides in Tetrahydrofuran by UV-Vis, Fluorescence and ESR Spectroscopy. *Inorg. Chem. Acta* **1988,** *144*, 143-146.

7. Rice, N. T.; Su, J.; Gompa, T. P.; Russo, D. R.; Telser, J.; Palatinus, L.; Bacsa, J.; Yang, P.; Batista, E. R.; La Pierre, H. S., Homoleptic Imidophosphorane Stabilization of Tetravalent Cerium. *Inorg. Chem.* **2019,** *58*, 5289-5304.

8. Windorff, C. J.; Dumas, M. T.; Ziller, J. W.; Gaunt, A. J.; Kozimor, S. A.; Evans, W. J., Small-Scale Metal-Based Syntheses of Lanthanide Iodide, Amide, and Cyclopentadienyl Complexes as Analogues for Transuranic Reactions. *Inorg. Chem.* **2017,** *56*, 11981-11989.

9. Johnson, S. A.; Kiernicki, J. J.; Fanwick, P. E.; Bart, S. C., New Benzylpotassium Reagents and Their Utility for the Synthesis of Homoleptic Uranium(IV) Benzyl Derivatives. *Organometallics* **2015,** *34*, 2889-2895.

10. Fetz, M.; Gerber, R.; Blacque, O.; Frech, C. M., Hydrolysis of Ammonia Borane Catalyzed by Aminophosphine-Stabilized Precursors of Rhodium Nanoparticles: Ligand Effects and Solvent-Controlled Product Formation. *Chem. Eur. J.* **2011,** *17*, 4732-4736.

11. Dolomanov, O. V.; Bourhis, L. J.; Gildea, R. J.; Howard, J. A. K.; Puschmann, H., OLEX2: A Complete Structure Solution, Refinement and Analysis Program. *J. Appl. Cryst.* **2009,** *42*, 339-341.

12. Sheldrick, G. M., SHELXT - Integrated Space-Group and Crystal-Structure Determination. *Acta Cryst.* **2015,** *A71*, 3-8.

13. Sheldrick, G. M., Crystal Structure Refinement with SHELXL. *Acta Cryst.* **2015,** *C71*, 3-8.